Universität Hamburg
DER FORSCHUNG | DER LEHRE | DER BILDUNG

hamburger sternwarte

Master's Thesis

Main Sequence Binary Evolution Towards Double Detonation Supernovae

Author
Sumit Kumar Maheshwari

Department: Department of Physics

Degree Programme: MSc Physics

Matriculation Number: 7826935

First Examiner: Prof. Thomas Kupfer

Second Examiner: Dr. Mercedes Hernandez

Abstract

This master's thesis investigates the evolutionary pathway of binary systems that can lead to Type Ia supernovae through the double-detonation mechanism. The study focuses on the "sdB-first" channel, in which an initially more massive star loses its hydrogen-rich envelope through stable Roche-lobe overflow and becomes a hot subdwarf B (sdB) star, before its companion subsequently evolves into a carbon–oxygen white dwarf through a common envelope phase. This evolutionary sequence is motivated by the observed properties of compact sdB+WD systems proposed as progenitors of double-detonation supernovae, in which the sdB is the older component.

Using numerical binary-evolution calculations with the MESA code, a grid of 106,428 main sequence binary systems was computed to determine the initial conditions and mass-transfer properties that can produce compact sdB+WD systems. The resulting progenitors preferentially originate from binaries with intermediate-mass primary stars, mass ratios close to unity, and initial orbital periods of a few days. The study further reconstructs the progenitor systems of CD$-30°11223$ by combining the observed component masses and the orbital period inferred from its evolutionary history.

The reconstructed systems provide constraints on the mass-transfer efficiency β during the first interaction and the common envelope efficiency $\alpha_{\rm CE}$ during the second interaction. The resulting $\alpha_{\rm CE}$ values are generally higher than those inferred for white dwarf–main sequence post-common envelope binaries, indicating that the efficiency of common envelope ejection may depend on the evolutionary properties of the donor and cannot necessarily be described by a universal value. Overall, this work demonstrates the physical viability of the sdB-first channel and provides a framework for estimating thermonuclear supernova rates in the Galaxy.

Acknowledgements

I would like to thank my supervisors, Prof. Thomas Kupfer and Dr. Mercedes Hernandez, for their guidance and support throughout this thesis. They not only introduced me to the physics of main-sequence binary evolution and double-detonation supernovae, but also taught me key aspects of conducting research: asking precise questions, interpreting numerical results critically, and communicating scientific ideas. Their encouragement and the independence they gave me to explore the project allowed me to develop skills that I will carry into future work.

I am also grateful to the *Regionales Rechenzentrum* (RRZ) of Universität Hamburg for providing access to the Hummel 2 high-performance computing cluster and for their technical support in running the simulations. Their assistance in diagnosing and resolving computational issues was essential for completing the large MESA grid used in this thesis.

Finally, I would like to thank my family for their unwavering support throughout my studies. Their patience, encouragement, and belief in me have been crucial in allowing me to complete this thesis. This work would not have been possible without their constant help and trust.

Contents

Abstract i

Acknowledgements ii

1 Introduction 1

1.1 White dwarfs . . . 2
1.1.1 Electron degeneracy pressure . . . 3
1.1.2 Composition and evolution . . . 5
1.2 Type Ia supernovae . . . 7
1.2.1 Radioactive powering and the Phillips relation . . . 9
1.3 Progenitor channels of Type Ia supernovae . . . 12
1.3.1 Single-degenerate . . . 13
1.3.2 Double-degenerate . . . 14
1.3.3 Sub-Chandrasekhar explosion channels . . . 14
1.3.4 Comparison of progenitor channels . . . 15
1.4 Double-detonation pathway . . . 15
1.4.1 Physical mechanism . . . 16
1.4.2 helium shell ignition and detonation . . . 16
1.4.3 Triggering the CO-core detonation . . . 17
1.4.4 Dependence on WD/shell mass . . . 18
1.4.5 Observational predictions . . . 18
1.4.6 Helium-rich donor stars . . . 19
1.5 Hot subdwarf B stars . . . 20
1.5.1 Structure and evolutionary properties . . . 20
1.5.2 Formation channels . . . 23
1.5.3 Common envelope evolution . . . 24
1.5.4 Evolution after core-helium burning . . . 26
1.6 sdB+WD binaries . . . 26
1.6.1 Formation of compact sdB+WD systems . . . 26

1.6.2 Characteristic timescales . . . 27
1.6.3 Helium mass transfer and future evolution . . . 29
1.6.4 Known double-detonation progenitor candidates . . . 30
1.7 Goal of the Thesis . . . 31

2 Methodology **32**
2.1 Evolutionary Pathways for AM CVn . . . 32
2.1.1 Classical Pathway . . . 32
2.1.2 Alternate Pathway (sdB-First) . . . 35
2.1.3 Pathway for CD-30°11223 . . . 36
2.2 Modeling and Simulations . . . 36
2.2.1 Simulation Setup . . . 37
2.2.2 sdB formation through stable mass transfer . . . 38
2.2.3 White Dwarf formation through common envelope . . . 39

3 MESA Grid and Analysis **41**
3.1 Grid of Simulations . . . 41
3.2 Selection Procedure . . . 43
3.3 Successful Candidates/Systems . . . 44
3.3.1 2D Histogram of Period vs Primary Mass . . . 44
3.3.2 Initial Mass Space . . . 46
3.3.3 Parameters Distribution . . . 47

4 CD-30 Progenitors **50**
4.1 sdB and WD Mass Constraints . . . 50
4.2 Identification of CD-30°11223 Progenitor Systems . . . 52
4.3 Mass Space of Candidates . . . 54
4.4 Distributions of CD-30 progenitors . . . 55
4.5 Initial Period vs β . . . 57
4.6 sdB and WD Evolution . . . 58
4.7 α_{CE} Constraint . . . 60
4.8 Discussion . . . 61
4.8.1 common envelope Efficiency . . . 61
4.8.2 Connection to Double-detonation Progenitors . . . 64

5 Conclusions and Future Directions **66**
5.1 Conclusions . . . 66
5.2 Future Directions . . . 68
5.2.1 Classification of new candidates . . . 68

5.2.2 Constraining the double-detonation rate 68
5.2.3 Sensitivity to model assumptions 68
5.2.4 Broader observational use 69

References **70**

A Additional Material **80**
A.1 CD-30 Progenitors List 80
A.2 Inlist Files for MESA Simulations 82
A.2.1 Inlist_project 82
A.2.2 Inlist_1 85
A.2.3 Inlist_2 91

Statutory Declaration **95**

List of Figures

1.1 Schematic evolution of a 1 $M_\odot$ star from the zero-age main sequence to the white dwarf stage. The evolutionary phases include the sub-giant branch, red-giant branch, horizontal branch, asymptotic giant branch, post-AGB evolution, and white dwarf cooling. Reproduced from Carroll and Ostlie (2006). 3

1.2 Gaia H–R diagrams showing different white dwarf populations. Reproduced from Gentile Fusillo et al. (2019). 7

1.3 Representative Type Ia supernova light curves. Adapted from Hamuy et al. (1996). 8

1.4 The Phillips luminosity–decline-rate relation for Type Ia supernovae. Adapted from Phillips (1993); Phillips et al. (1999). 10

1.5 Type Ia supernova diversity in the Phillips diagram. Adapted from (Taubenberger, 2017) 11

1.6 Schematic representation of the double-detonation mechanism. Adapted from (Fink et al., 2010) 17

1.7 Location of hot subdwarf B stars on the extreme horizontal branch. Adapted from Heber (2009). 21

1.8 Evolutionary sequence of the binary system considered in this thesis, showing the formation of the sdB through stable Roche-lobe overflow and the subsequent common envelope phase. 22

2.1 The Classical Evolution of AM CVn stars 33

2.2 The Alternate Channel for AM CVn stars 35

3.1 Selection Procedure 43

3.2 2D Histogram for period vs primary mass 45

3.3 Mass Space of successful systems 46

3.4 Parameter Distribution 48

4.1 sdB and WD mass distribution 51

4.2 Example of the progenitor selection procedure for a representative binary model. The blue curve shows the post-common envelope orbital period predicted by the model as a function of the common envelope efficiency parameter, $\alpha_{\rm CE}$. The horizontal dashed line represents the reconstructed post-common envelope orbital period of CD-30°11223 ($P_{\rm CE,cool} = 88.7\,{\rm min}$), while the vertical dashed line indicates the value of $\alpha_{\rm CE}$ that provides the closest match. This procedure was repeated for every simulated binary to identify viable progenitor systems of CD-30°11223. 53
4.3 Mass Space of the possible progenitors of CD-30 54
4.4 Parameter distribution of CD-30 progenitors 56
4.5 Initial Period and β distribution of the candidates as a function of α & β 58
4.6 M2 and M1 evolution for the candidates as a function of β 59
4.7 Constraint on CE Efficiency for the CD-30 Progenitors 60

List of Tables

3.1 Parameter ranges explored in the MESA binary evolution grid. 41

A.1 Initial parameters of the 53 viable CD-30°11223 progenitor candidates. 80

Chapter 1

Introduction

Type Ia supernovae are thermonuclear explosions that play a central role in astrophysics. They contribute to the chemical enrichment of galaxies and, through their calibrated luminosities, provide key measurements of the expansion history of the Universe. Despite their importance, the binary systems and evolutionary processes that lead to these explosions remain uncertain (Howell, 2011; Maoz et al., 2014). In the double-detonation scenario, a carbon–oxygen white dwarf accretes helium from a companion and may explode below the Chandrasekhar mass after helium shell ignition triggers a second detonation in the CO core. Compact binaries containing a hot subdwarf B star and a white dwarf are relevant to this scenario because the sdB star can act as a helium rich donor after the binary orbit has been reduced by gravitational wave emission (Geier et al., 2013; Heber, 2009).

The present-day properties of an sdB+WD binary do not uniquely determine how it formed. They depend on the initial stellar masses, the initial orbital separation, the stability and efficiency of the first mass-transfer phase, and the outcome of later common envelope evolution (Han et al., 2002a). Reconstructing this history is therefore necessary to connect observed compact binaries to the double-detonation progenitor population. This thesis investigates the sdb-first formation channel, motivated by observations of compact sdB+WD systems proposed as progenitors of sub-Chandrasekhar double-detonation SNe Ia, for which the sdB has been found to be the older component of the binary (Hernandez et al., 2026; Kupfer et al., 2022). This chapter develops the physical background needed for that investigation. It first introduces white dwarfs and their internal structure, composition, cooling, and observational classification. It then discusses Type Ia supernovae, their observational properties and use as distance indicators, followed by the proposed progenitor channels and the double-detonation pathway. The chapter next introduces hot subdwarf B stars and compact sdB+WD binaries, including their characteristic evolutionary

timescales and future helium-transfer evolution. Finally, the prototypical system CD-30°11223 is discussed in detail, followed by the objectives of reconstructing its main-sequence progenitors.

1.1 White dwarfs

White dwarfs (WDs) are the compact remnants produced by the evolution of the vast majority of low- and intermediate-mass stars (Koester, 2013). After the exhaustion of their nuclear fuel, these stars lose most of their envelopes during the red-giant and asymptotic-giant-branch phases, leaving behind a degenerate stellar core. More than $\sim 95\%$ of stars are expected to end their evolution as white dwarfs rather than as neutron stars or black holes (Bédard, 2024). The formation of a white dwarf is therefore primarily a problem of envelope removal and core growth rather than of continued nuclear burning. The final mass of the remnant retains information about the previous evolution of the progenitor and is described observationally by the initial–final mass relation (Gentile Fusillo et al., 2019).

A schematic evolutionary sequence from the zero-age main sequence to the white dwarf stage is shown in Fig. 1.1. The evolutionary path includes the subgiant and red-giant branches, core helium burning, asymptotic-giant-branch evolution, post-AGB evolution, and finally the white dwarf cooling sequence. During the giant phases, the stellar envelope can be removed through stellar winds or binary interaction, exposing a degenerate core. In a binary system, mass transfer, Roche-lobe overflow, and common envelope evolution can remove the envelope much more efficiently than single-star mass loss. This binary channel is important for the formation of low-mass white dwarfs and for the production of compact binaries.

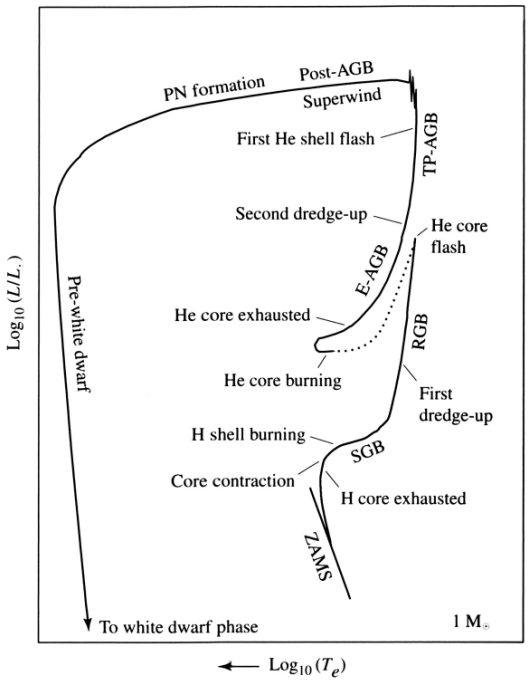


Figure 1.1: Schematic evolution of a $1\,M_\odot$ star from the zero-age main sequence to the white dwarf stage. The evolutionary phases include the subgiant branch, red-giant branch, horizontal branch, asymptotic giant branch, post-AGB evolution, and white dwarf cooling. Reproduced from Carroll and Ostlie (2006).

The final mass of a white dwarf is closely connected to the initial mass of its progenitor. This relation is not one-to-one in a simple stellar-evolution sense because substantial mass is lost during the giant phases. Empirical initial–final mass relations derived from white dwarfs in star clusters and wide binaries show that the final mass increases with progenitor mass, but with a non-linear relation and significant sensitivity to the details of stellar evolution (Gentile Fusillo et al., 2019). The typical mass of a field white dwarf is around $0.6\,M_\odot$, while the observed distribution extends from extremely low-mass objects produced predominantly through binary evolution to massive white dwarfs approaching the Chandrasekhar limit (Bédard, 2024; Gentile Fusillo et al., 2019). The distinction between these populations is important because the mass determines the radius, central density, cooling rate, and ultimately the conditions required for thermonuclear ignition.

1.1.1 Electron degeneracy pressure

The defining physical property of a white dwarf is that its hydrostatic support is provided predominantly by electron degeneracy pressure. As the progenitor core contracts after nuclear burning, the density becomes high enough that the electrons

occupy quantum states up to the Fermi energy. The Pauli exclusion principle prevents electrons from occupying identical quantum states, and the resulting Fermi momentum produces a pressure even when the temperature contribution to the pressure is negligible.

For an electron number density $n_{\rm e}$, the Fermi momentum is

$$p_{\rm F} = \hbar (3\pi^2 n_{\rm e})^{1/3}, \tag{1.1}$$

where

$$n_{\rm e} = \frac{\rho}{\mu_{\rm e} m_{\rm u}}, \tag{1.2}$$

with ρ the mass density, $\mu_{\rm e}$ the mean molecular weight per electron, and $m_{\rm u}$ the atomic mass unit. The degeneracy pressure has two limiting forms. When the electrons are non-relativistic,

$$P_{\rm e} = \frac{\hbar^2}{5 m_{\rm e}} (3\pi^2)^{2/3} \left(\frac{\rho}{\mu_{\rm e} m_{\rm u}} \right)^{5/3}, \tag{1.3}$$

so that

$$P_{\rm e} \propto \rho^{5/3}. \tag{1.4}$$

At sufficiently high densities the electrons become relativistic and the equation of state approaches

$$P_{\rm e} = \frac{\hbar c}{4} (3\pi^2)^{1/3} \left(\frac{\rho}{\mu_{\rm e} m_{\rm u}} \right)^{4/3}, \tag{1.5}$$

giving

$$P_{\rm e} \propto \rho^{4/3}. \tag{1.6}$$

This transition from a 5/3 to a 4/3 polytropic relation is fundamental to the existence of a limiting white dwarf mass. Combining the relativistic degeneracy equation of state with hydrostatic equilibrium gives the Chandrasekhar mass,

$$M_{\rm Ch} \simeq \frac{5.83}{\mu_{\rm e}^2} \, M_\odot. \tag{1.7}$$

For a C/O composition, $\mu_{\rm e} \simeq 2$, giving a value close to $1.4\, M_\odot$. The precise limiting mass is modified by Coulomb corrections, finite-temperature effects, rotation, general relativity, and the detailed composition of the star (Chandrasekhar, 1939).

The Chandrasekhar limit should not be interpreted as the typical mass of a white dwarf. Most white dwarfs are substantially below this limit. It represents the maximum mass of a cold, non-rotating, electron-degenerate configuration for a specified composition. As the mass approaches this limit, the increasing importance of relativistic degeneracy causes the radius to decrease strongly while the central density increases. This property is especially important for thermonuclear explosions because the density of the C/O material determines the nuclear-burning products produced during a detonation.

The inverse dependence of radius on mass is another characteristic property of degenerate stars. In the non-relativistic limit, hydrostatic equilibrium and the relation $P_{\rm e} \propto \rho^{5/3}$ give approximately

$$R_{\rm WD} \propto M_{\rm WD}^{-1/3}. \tag{1.8}$$

Thus, adding mass to a white dwarf causes it to become smaller rather than larger. A more complete zero-temperature approximation can be written as

$$R_{\rm WD} \simeq 0.0112\, R_\odot \left[\left(\frac{M_{\rm Ch}}{M_{\rm WD}} \right)^{2/3} - \left(\frac{M_{\rm WD}}{M_{\rm Ch}} \right)^{2/3} \right]^{1/2}, \tag{1.9}$$

for a composition with $\mu_{\rm e} \simeq 2$. This expression shows both limiting behaviours: at low masses the radius approximately follows $M^{-1/3}$, whereas as $M_{\rm WD}$ approaches $M_{\rm Ch}$ the radius tends towards zero in the idealized zero-temperature model (Chandrasekhar, 1939).

Although a typical white dwarf has a mass comparable to that of the Sun, its radius is comparable to that of the Earth. Consequently,

$$g_{\rm WD} = \frac{G M_{\rm WD}}{R_{\rm WD}^2} \tag{1.10}$$

is extremely large, with typical surface gravities around $\log g \simeq 7.5$–9.0 in cgs units. The high surface gravity has important observational consequences. It produces strong pressure broadening of spectral lines and causes heavy elements to gravitationally settle out of the photosphere on timescales much shorter than the cooling age. As a result, the atmospheric composition of a white dwarf can be very different from the composition of the underlying degenerate core.

1.1.2 Composition and evolution

The evolutionary outcome of a star is primarily determined by its initial mass. Stars that lose their envelopes after core helium burning generally form carbon–

oxygen (CO) white dwarfs, while more massive progenitors that undergo carbon burning can produce oxygen–neon (ONe) white dwarfs. The boundary between these outcomes depends on factors such as metallicity, convective overshooting, rotation, and mass loss. For the double-detonation channel considered in this thesis, the relevant remnant is a CO white dwarf, whose core consists primarily of carbon and oxygen produced during core helium burning through the triple-α and $^{12}\mathrm{C}(\alpha,\gamma)^{16}\mathrm{O}$ reactions (Bédard, 2024; Gentile Fusillo et al., 2019).

A white dwarf is strongly stratified by gravitational settling. The heavy C/O core is surrounded by lighter helium and, where present, a thinner hydrogen layer. The electrons provide the pressure support, while the ions contain most of the thermal energy. The atmospheric composition can therefore evolve independently of the core composition. This distinction is important when interpreting observation because the spectral type describes the atmosphere and does not directly indicate the composition of the degenerate core (Bédard, 2024).

White dwarfs are classified spectroscopically according to their atmospheric features. DA white dwarfs have hydrogen-dominated atmospheres and broad Balmer absorption lines, while DB and DO stars are dominated by neutral and ionized helium, respectively. Other classes include DC objects with featureless spectra, DQ stars showing carbon features, and DZ stars showing metal lines. Magnetic fields and mixed atmospheric compositions are indicated by additional classification suffixes (Bédard, 2024; Gentile Fusillo et al., 2019; Koester, 2013).

After formation, a white dwarf has no substantial long-term nuclear energy source and evolves mainly by cooling. Its high electron conductivity makes the interior approximately isothermal, while the outer envelope regulates the loss of thermal energy. The cooling rate depends on the white dwarf mass, atmospheric composition, and internal physical processes such as neutrino emission and crystallization (Gentile Fusillo et al., 2019). These effects are important for understanding the observed white dwarf population, although the detailed cooling physics is not central to the binary-evolution calculations presented in this thesis.

The Gaia colour–magnitude diagram provides a direct view of the white dwarf population. White dwarfs form a distinct cooling sequence, with their position depending on temperature, atmospheric composition, and mass. The different cooling tracks in Fig. 1.2 demonstrate the dependence on mass, while the observed sequences show the separation between hydrogen- and helium-atmosphere populations. Less common objects, including magnetic, carbon-rich, metal-polluted, and binary white dwarfs, occupy other regions of the diagram (Gentile Fusillo et al., 2019).

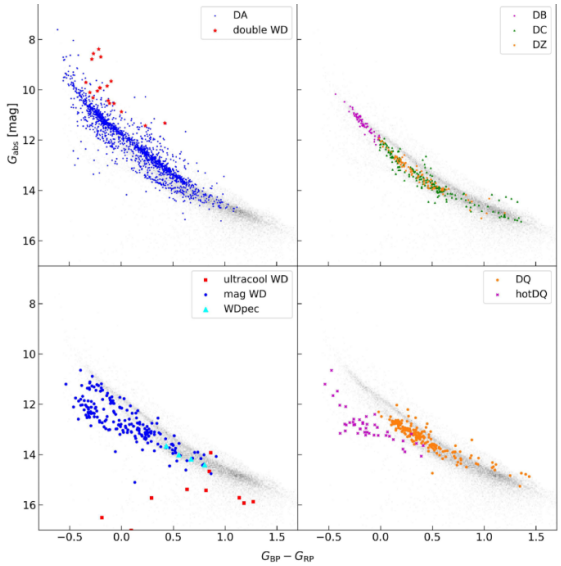


Figure 1.2: Gaia H–R diagrams showing different white dwarf populations. Reproduced from Gentile Fusillo et al. (2019).

Binary evolution can significantly alter the properties of white dwarfs. Envelope stripping through Roche-lobe overflow or common envelope evolution can produce low-mass helium-core remnants, while mergers and mass transfer can produce more massive white dwarfs. Close binaries are particularly relevant to the double-detonation scenario because they provide a mechanism for transferring helium-rich material onto a CO white dwarf. The mass and composition of the WD therefore provide important initial conditions for its later interaction with a helium-rich companion.

For the evolutionary channel studied in this thesis, the relevant object is a sub-Chandrasekhar CO white dwarf that can eventually accrete helium from an sdB donor. Its mass and internal composition determine the conditions under which the accreted helium can ignite and potentially trigger a subsequent detonation of the underlying CO core. The detailed double-detonation mechanism is discussed separately in Section 1.4.

1.2 Type Ia supernovae

Type Ia supernovae (SNe Ia) are thermonuclear explosions associated with carbon–oxygen (CO) white dwarfs. Unlike core-collapse supernovae, their energy is released by the explosive nuclear burning of degenerate stellar material instead by the gravitational collapse of a massive stellar core (Howell, 2011; Maoz et al., 2014). Near maximum light, normal SNe Ia show prominent absorption features from intermediate-mass elements, particularly Si, S, Ca, and Mg, while hydrogen is generally absent.

The strong Si II feature near 6355 Å is one of their characteristic spectroscopic signatures (Branch, 1998).

SNe Ia exhibit broadly similar light curves, with a rapid rise to maximum followed by a decline over several months. Their peak luminosities, decline rates, and spectra show significant diversity (Branch, 1998; Phillips, 1993). This diversity is important for the progenitor problem, although SNe Ia form a recognizable observational class, their properties do not uniquely identify a single explosion mechanism or progenitor channel.

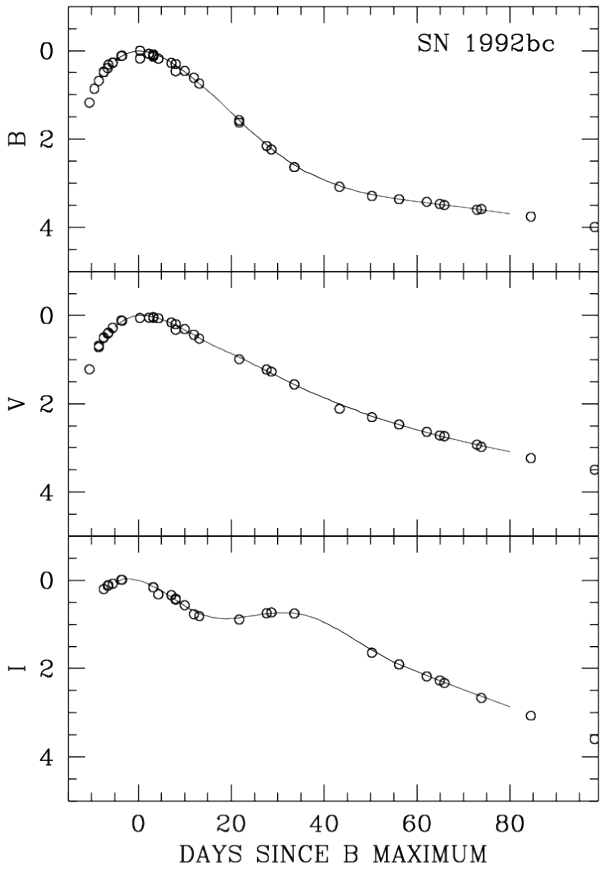


Figure 1.3: Representative Type Ia supernova light curves. Adapted from Hamuy et al. (1996).

Figure 1.3 shows the common overall evolution of SNe Ia while also showing differences in peak brightness and decline rate. These variations form the basis of the empirical luminosity–width relation discussed below.

1.2.1 Radioactive powering and the Phillips relation

The luminosity of a SN Ia is primarily powered by the radioactive decay of ^{56}Ni synthesized during the explosion. The decay chain

$$^{56}\mathrm{Ni} \rightarrow {}^{56}\mathrm{Co} \rightarrow {}^{56}\mathrm{Fe} \tag{1.11}$$

releases energy through gamma-rays and positrons, which heat the expanding ejecta. Consequently, the amount of ^{56}Ni produced during the explosion strongly influences the peak luminosity (Hillebrandt and Niemeyer, 2000).
The observed luminosity is also affected by the ejecta mass, opacity, expansion velocity, and distribution of radioactive material. These properties determine how efficiently the deposited radioactive energy can diffuse out of the expanding ejecta and therefore influence the width of the light curve.
The luminosity variation among SNe Ia is empirically correlated with the rate at which their light curves decline after maximum light (Phillips, 1993). This is commonly described using $\Delta m_{15}(B)$, defined as

$$\Delta m_{15}(B) = B(t_{\mathrm{max}} + 15\,\mathrm{d}) - B(t_{\mathrm{max}}). \tag{1.12}$$

Smaller values correspond to broader, more slowly declining and generally more luminous events, while larger values correspond to narrower and fainter light curves. The relation can be expressed schematically as

$$M_B = M_{B,0} + a\left[\Delta m_{15}(B) - \Delta m_{15,0}(B)\right], \tag{1.13}$$

where M_B is the peak absolute B-band magnitude and a is an empirical coefficient.

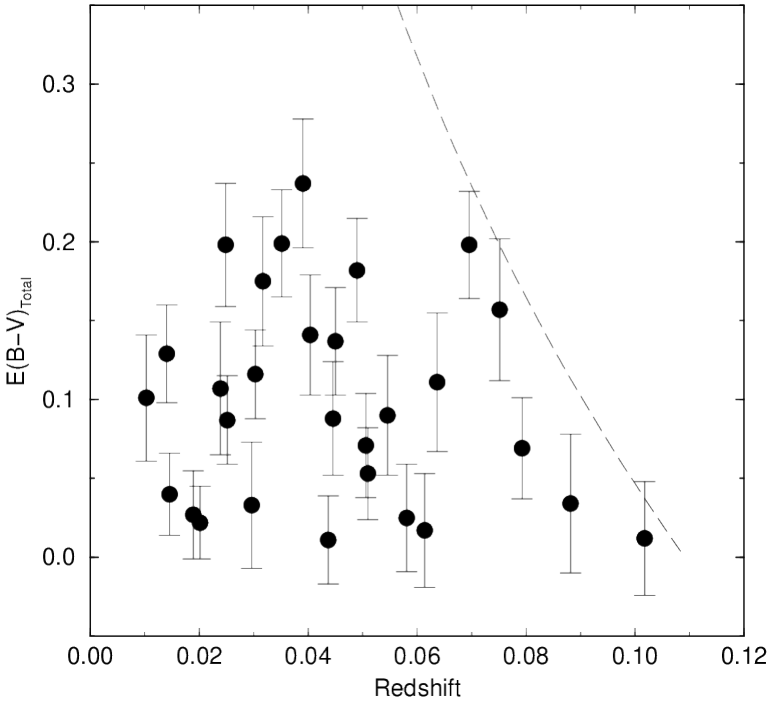


Figure 1.4: The Phillips luminosity–decline-rate relation for Type Ia supernovae. Adapted from Phillips (1993); Phillips et al. (1999).

Figure 1.4 shows the correlation between peak absolute magnitude and $\Delta m_{15}(B)$. The relation allows the luminosities of normal SNe Ia to be empirically standardized and explains why these events can be used as distance indicators. Though, it should be viewed as an empirical relation for a particular population and not as evidence that all thermonuclear supernovae arise from the same physical conditions.

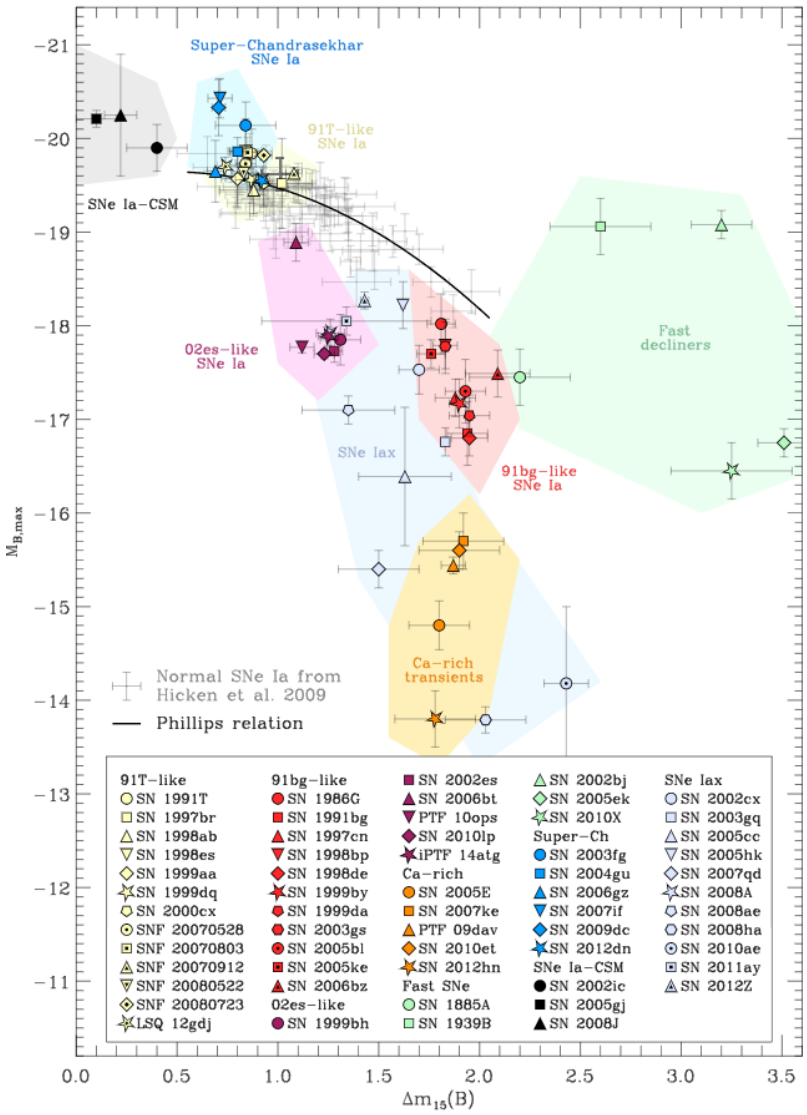


Figure 1.5: Type Ia supernova diversity in the Phillips diagram. Adapted from (Taubenberger, 2017)

Figure 1.5 places the Phillips relation in the context of the broader observed thermonuclear-supernova population. While normal SNe Ia occupy a relatively well-defined region around the Phillips relation, several subclasses show substantial deviations in peak luminosity and decline rate (Taubenberger, 2017). These include subluminous 91bg-like events, SNe Iax, super-Chandrasekhar candidates, 91T-like events, and other peculiar thermonuclear transients. The figure therefore demonstrates that the Phillips relation is an effective description of the normal SN Ia population, but it does not provide a universal description of all thermonuclear explosions. The presence of objects that are significantly brighter or fainter than expected from their decline rate indicates that their explosion physics and/or progenitor properties can differ

from those of normal SNe Ia. This motivates considering alternative progenitor and explosion channels rather than restricting the discussion to the population that follows the standard luminosity–decline-rate relation. For this thesis, this distinction is important because sub-Chandrasekhar explosions, including the double-detonation channel, provide a physically distinct route to thermonuclear explosions and do not require a Chandrasekhar-mass white dwarf. Understanding these alternative channels therefore provides the necessary connection between the observed diversity of thermonuclear supernovae and the binary evolutionary pathway investigated in this work.

1.3 Progenitor channels of Type Ia supernovae

The proposed progenitor scenarios can be broadly divided according to the nature of the companion to the exploding white dwarf and the manner in which thermonuclear ignition is achieved. The classical categories are the single-degenerate (SD) and double-degenerate (DD) scenarios, while sub-Chandrasekhar explosion mechanisms, particularly the double-detonation scenario, provide an additional class of pathways in which the white dwarf does not need to approach the Chandrasekhar mass (Hillebrandt and Niemeyer, 2000; Maoz et al., 2014).

Despite decades of theoretical and observational work, the binary systems that produce the majority of SNe Ia have not been uniquely identified. The central problem is that the explosion occurs long after the progenitor system was formed, and the pre-explosion binary can undergo one or more phases of mass transfer, common envelope evolution, merger, or orbital decay.

The observed SN Ia rate provides an additional constraint. The delay between the formation of a stellar population and the subsequent SN Ia explosion can range from tens of millions of years to several billion years. Observed SN Ia rates are broadly consistent with a delay-time distribution that declines approximately as a power law,

$$\mathrm{DTD}(t) \propto t^{-1}, \tag{1.14}$$

although the exact normalization and minimum delay time remain subjects of active investigation (Maoz and Graur, 2017; Maoz et al., 2014). Independent measurements based on supernova remnants in the Magellanic Clouds confirm a similar prompt component within a few hundred million years of star formation (Maoz and Badenes, 2010).

This broad range of delay times is difficult to reconcile with a single, simple evo-

lutionary pathway. Instead, it suggests that several types of binary systems may contribute to the observed SN Ia population. The progenitor problem is therefore closely related to binary stellar evolution as different binary configurations can produce different routes to the thermonuclear ignition of a CO white dwarf.

1.3.1 Single-degenerate

In the single-degenerate scenario, a CO white dwarf is accompanied by a non-degenerate star. The donor may be a main-sequence star, subgiant, red giant, or helium-rich star. Mass transfer through Roche-lobe overflow or stellar winds supplies material to the white dwarf.
If the accretion rate lies in an appropriate regime, hydrogen-rich material can burn relatively steadily on the WD surface. The resulting helium layer can subsequently undergo helium burning, the white dwarf may retain a fraction of the accreted material and increase in mass.
The classical Chandrasekhar-mass version of the SD channel requires the WD to grow towards approximately

$$M_{\mathrm{Ch}} \simeq 1.4\, M_{\odot}. \tag{1.15}$$

As the central density increases, carbon ignition can occur under strongly degenerate conditions. Because the pressure of the degenerate electrons is only weakly dependent on temperature, nuclear heating is not efficiently balanced by expansion. The resulting thermonuclear runaway can hence disrupt the white dwarf.
Several observational searches have tested this scenario. These include searches for surviving companions, circumstellar material, supersoft X-ray sources, and signatures of interaction between SN ejecta and pre-existing stellar material. Deep pre-explosion imaging of nearby events such as SN 2011fe has excluded luminous red-giant companions (Li et al., 2011), and searches for surviving ex-companion stars in resolved supernova remnants, including SNR 0509−67.5, have likewise found no evidence of a surviving non-degenerate donor (Schaefer and Pagnotta, 2012). Population-synthesis calculations further show that the predicted rate of Chandrasekhar-mass SD explosions falls short of the observed SN Ia rate (Ruiter et al., 2009). Although some observations are compatible with SD systems, no single observational test has established the SD channel as the dominant source of all SNe Ia (Maoz et al., 2014).

1.3.2 Double-degenerate

The double-degenerate scenario consists of two white dwarfs in a compact binary. The system loses orbital energy and angular momentum through gravitational wave emission, causing the orbit to shrink. The gravitational wave driven evolution is described, in the point-mass approximation, by

$$\frac{da}{dt} = -\frac{64}{5}\frac{G^3 M_1 M_2 (M_1 + M_2)}{c^5 a^3}. \tag{1.16}$$

If the binary becomes sufficiently compact, the less massive WD can begin mass transfer to its companion. Depending on the mass ratio, the donor's response, and the hydrodynamic interaction between the two stars, the system may undergo stable mass transfer, a merger, or a dynamically violent interaction.

A merger involving two CO white dwarfs can potentially produce a thermonuclear explosion. In the violent-merger interpretation, carbon burning can be initiated during the dynamical interaction itself, and three-dimensional simulations of such violent mergers have shown that sufficiently massive WD pairs can reproduce the light curves and spectra of normal-brightness SNe Ia rather than only sub-luminous events (Pakmor et al., 2012). In other models, the merger produces a differentially rotating or hot remnant that subsequently evolves toward ignition.

The DD channel is attractive because it naturally produces long delay times and does not require the survival of a non-degenerate companion until the explosion but not every WD merger necessarily produces a SN Ia. Depending on the component masses, mass ratio, composition, and thermal state, the outcome may instead be a stable remnant or collapse toward a neutron star. Consequently, the merger process and the conditions for thermonuclear ignition remain important theoretical questions (Kromer et al., 2010; Pakmor et al., 2010).

1.3.3 Sub-Chandrasekhar explosion channels

An important alternative to Chandrasekhar-mass explosion scenarios is that a CO white dwarf can undergo a thermonuclear explosion before reaching the Chandrasekhar limit. Such models are attractive because they allow the explosion to occur in a WD with a mass substantially below $M_{\rm Ch}$.

The principal mechanism considered in this thesis is the double-detonation scenario. In this model, the CO white dwarf accumulates a helium-rich layer on its surface. Under sufficiently degenerate conditions, the helium layer can ignite unstably and transition to a detonation. The resulting shock and compression can then initiate a second detonation in the underlying carbon–oxygen material.

The important distinction is therefore

$$\boxed{\text{Chandrasekhar-mass ignition} \neq \text{sub-Chandrasekhar double detonation.}} \quad (1.17)$$

In the former, the central carbon ignition is associated with a WD approaching the Chandrasekhar mass. In the latter, the WD explodes at a lower mass because a surface helium detonation provides the trigger for the core explosion.

1.3.4 Comparison of progenitor channels

The proposed progenitor scenarios differ in both their evolutionary pathways and in the physical conditions under which thermonuclear ignition is achieved. The single-degenerate channel requires a non-degenerate companion and, in its classical form, growth of the WD towards the Chandrasekhar mass. The double-degenerate channel involves two WDs and generally relies on merger or dynamical interaction. Sub-Chandrasekhar channels instead allow the CO WD to explode below the Chandrasekhar mass, with the double-detonation mechanism providing a natural route when helium is supplied by a compact helium-rich donor. These scenarios are not necessarily mutually exclusive in terms of their observable outcomes, and their relative contributions to the SN Ia population remain uncertain.
The broad delay-time distribution and the diversity of observed SN Ia properties provide constraints on the relative importance of these channels, but neither uniquely identifies the dominant progenitor pathway. This uncertainty motivates focusing on physically testable evolutionary sequences for which compact progenitor systems can be identified observationally. The sdB+WD systems discussed below provide such a connection between a specific binary configuration and the sub-Chandrasekhar double-detonation mechanism.

1.4 Double-detonation pathway

The double-detonation scenario provides a direct connection between sub-Chandrasekhar CO white dwarfs and helium-rich donor stars. It was originally investigated as a mechanism in which a helium detonation occurs on the surface of a white dwarf and subsequently triggers a second detonation in the underlying CO core. Modern hydrodynamical calculations have shown that a helium shell detonation can, under suitable conditions, launch sufficiently strong shocks into the CO core to initiate a secondary detonation (Fink et al., 2010).

1.4.1 Physical mechanism

The double-detonation pathway begins with a sub-Chandrasekhar CO white dwarf that accumulates helium-rich matter. The essential sequence is the formation of a helium shell, unstable helium ignition and detonation, propagation of the helium detonation around the WD surface, and subsequent compression and ignition of the underlying CO core. The mechanism differs fundamentally from a Chandrasekhar-mass central ignition scenario because the initial trigger originates in the surface helium layer.

1.4.2 helium shell ignition and detonation

The donor can be a helium white dwarf, a helium star, or a hot subdwarf B star. The transferred helium accumulates on the surface of the CO white dwarf.
The thermal state of the accumulating helium layer depends strongly on the mass-transfer rate. At sufficiently high accretion rates, helium burning can proceed relatively steadily. At lower accretion rates, the helium layer can become increasingly degenerate. Continued accumulation then increases the pressure and temperature at the base of the shell.
Because degenerate pressure is only weakly dependent on temperature, a local increase in temperature does not necessarily produce rapid expansion and cooling. Nuclear burning can consequently become unstable. The helium burning rate increases strongly with temperature, producing a thermonuclear runaway.
For a sufficiently massive and degenerate helium shell, the burning can transition into a detonation. A detonation differs from a deflagration in that the burning front propagates supersonically and is driven by a shock wave. The detonation sweeps through the helium shell and releases a large amount of nuclear energy on a short timescale.
The minimum helium shell mass required for dynamical burning depends on the WD mass, shell composition, temperature, and degree of degeneracy, and was first quantified by Shen and Bildsten (2009), who calculated the shell mass at which the local helium burning timescale becomes shorter than the local dynamical timescale as a function of WD core mass. This minimum mass is naturally reached in AM CVn binaries, in which a CO WD accretes helium at a high rate from a degenerate or semi-degenerate helium-rich companion (Bildsten et al., 2007), making such systems natural candidate sites for helium shell detonations. It is therefore not a universal value. The presence of carbon, oxygen, or other contaminants in the helium layer can modify the nuclear reaction network and the conditions required for detonation.

Hydrodynamic calculations by Fink et al. (2010) demonstrated that a helium detonation can trigger a secondary detonation in the underlying CO core for a broad range of core and shell masses. Their calculations included WD core masses ranging from approximately 0.81 to 1.38 $M_{\odot}$, with corresponding helium shell masses ranging from approximately 0.13 to 0.004 $M_{\odot}$.

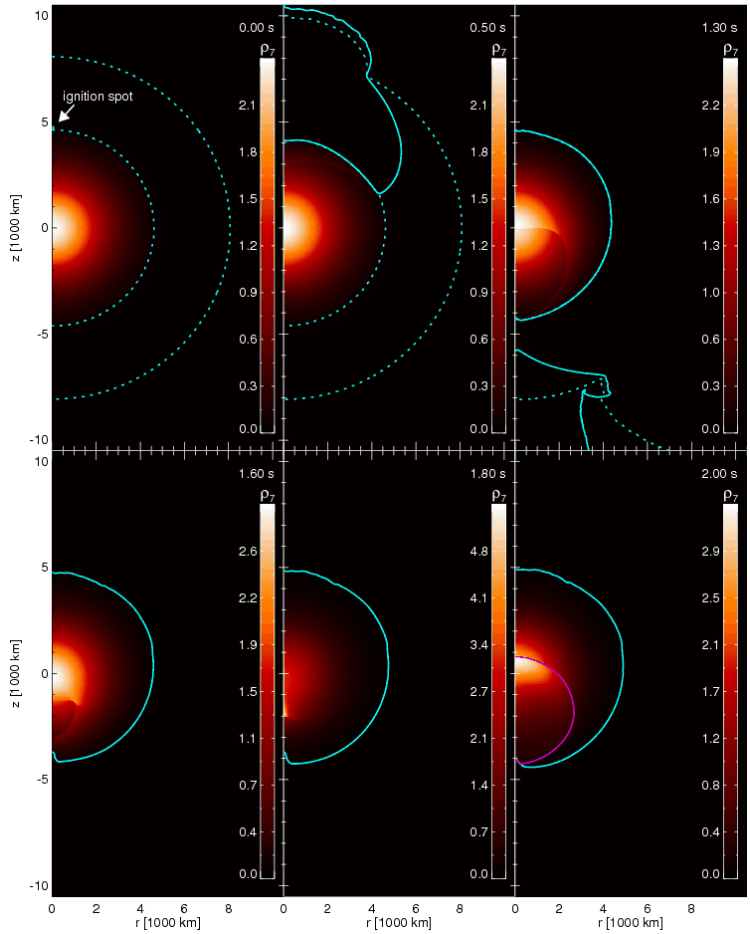


Figure 1.6: Schematic representation of the double-detonation mechanism. Adapted from (Fink et al., 2010)

Fig 1.6 shows a CO white dwarf surrounded by an accumulated helium shell. Ignition of the helium layer produces a detonation that propagates around the surface. The associated shock waves converge into the underlying CO core and can initiate a secondary CO detonation. The two detonations together disrupt the sub-Chandrasekhar white dwarf.

1.4.3 Triggering the CO-core detonation

The second stage of the mechanism is the triggering of a detonation in the CO core. As the helium detonation propagates around the WD surface, it generates shock

waves that penetrate the underlying material. These shocks compress and heat the CO core.
If the thermodynamic conditions in the compressed CO material become sufficient for rapid carbon burning, a secondary detonation can form. The result is a supersonic burning front propagating through the CO core and converting a substantial fraction of the carbon and oxygen into intermediate-mass and iron-group elements. The resulting explosion releases an energy of order

$$E_{\mathrm{nuc}} \sim 10^{51}\,\mathrm{erg}, \tag{1.18}$$

sufficient to overcome the gravitational binding energy of the WD and completely disrupt the star.

1.4.4 Dependence on WD/shell mass

The outcome of a double detonation depends on both the CO-core mass and the helium shell properties. A more massive CO white dwarf has a larger central density and generally produces a larger amount of iron-group material when detonated. The helium shell mass affects both the conditions required for ignition and the composition of the outer ejecta.
Early double-detonation models often considered relatively massive helium shells. Such models can produce substantial amounts of radioactive iron-group material in the outer ejecta, potentially producing spectral features that are inconsistent with normal SNe Ia. Modern calculations have explored much thinner helium shells, which can reduce the amount of helium burning ash in the outer ejecta while still allowing the core detonation to occur (Fink et al., 2010; Kasen et al., 2011; Polin et al., 2019).
This distinction is important for the interpretation of observed SNe Ia. The relevant question is not simply whether a helium shell can detonate, but whether a helium shell with a physically plausible composition and mass can produce an explosion whose nucleosynthetic yields, spectra, colours, and light curves resemble the observed SN Ia population.

1.4.5 Observational predictions

The double-detonation mechanism makes several observational predictions. Because the helium shell is burned before the CO core, the outermost ejecta can contain products of helium burning, including intermediate-mass and iron-group elements. The amount of these products depends strongly on the shell mass and composition.

The CO-core detonation produces the radioactive ^{56}Ni responsible for much of the optical luminosity. Consequently, the final luminosity and light-curve width depend strongly on the mass of the CO WD. More massive sub-Chandrasekhar WDs generally synthesize more ^{56}Ni and produce brighter explosions, while lower-mass WDs can produce fainter and faster evolving transients (Kasen et al., 2011; Polin et al., 2019).

The predicted spectra also depend on the helium shell mass. Thick helium shells can leave large amounts of helium burning products in the outer ejecta, producing strong high-velocity features. Thin-shell models can produce spectra more similar to normal SNe Ia, particularly for relatively massive CO WDs.

Thus, the double-detonation model provides a physical connection between three quantities:

$$M_{\rm WD} \quad \longrightarrow \quad M_{\rm Ni} \quad \longrightarrow \quad L_{\rm peak}, \tag{1.19}$$

while the helium shell mass and composition influence the outer ejecta and therefore the detailed spectra and colours. Interestingly, recent observations of the supernova remnant SNR 0509-67.5 in the Large Magellanic Cloud have provided the first confirmed candidate of a double detonation mechanism. Deep spectroscopy and imaging with Very Large Telescope (VLT) reveal concentric shells of calcium and other element whose spatial and abundance distribution are only reproduced by models in which a near surface helium detonation triggers CO core explosion (Mandal et al., 2026).

1.4.6 Helium-rich donor stars

A crucial requirement of the double-detonation scenario is a source of helium-rich material. Several donor configurations have therefore been considered, including helium white dwarfs, helium stars, and hot subdwarf stars.

The donor must satisfy two conditions. First, **it must contain sufficient helium to supply the accumulating shell**. Second, **the binary must reach a configuration in which mass transfer occurs at a rate compatible with helium shell accumulation and ignition**.

This requirement makes compact **helium star–CO WD binaries** very interesting. A hot subdwarf B star contains a helium burning core surrounded by only a thin hydrogen-rich envelope. If such a star is placed in a compact binary with a CO WD, gravitational wave radiation can gradually reduce the orbital separation until the sdB fills its Roche lobe. The followed transfer of helium-rich material can then

provide the fuel required for the double-detonation pathway.
This evolutionary connection provides the motivation for studying compact sdB+WD binaries. The double-detonation mechanism itself occurs only after the formation of the sdB+WD system; the formation of that compact binary is a separate binary-evolution problem. Determining which main-sequence binaries can evolve into the observed sdB+WD configuration requires reconstructing the earlier mass-transfer and common envelope phases.
The present work focuses on the evolutionary history of CD-30°11223. The observed system contains an sdB star and a CO white dwarf and has orbital properties that make it a strong candidate for future helium transfer and a double-detonation explosion. The next step is therefore to understand how such an sdB+WD system can be produced from an initially detached main-sequence binary.

1.5 Hot subdwarf B stars

1.5.1 Structure and evolutionary properties

Hot subdwarf B (sdB) stars are compact, hot stars undergoing core-helium burning on the extreme horizontal branch (EHB). They are the stripped remnants of red-giant stars that have lost most of their hydrogen-rich envelopes before or around the onset of helium burning. Consequently, an sdB consists predominantly of a helium burning core surrounded by a very thin hydrogen-rich envelope. Typical sdBs have effective temperatures of approximately 20,000–40,000 K, surface gravities of $\log g \simeq 5$–6.5, and masses close to the core mass required for helium ignition, typically around $0.47\,M_\odot$ (Han et al., 2002a; Heber, 2009; Saffer et al., 1994).
The characteristic mass of an sdB is set primarily by the helium core. During red-giant evolution, hydrogen-shell burning increases the core mass until it approaches the value required for helium ignition. If the hydrogen-rich envelope is removed at this stage, the exposed core can ignite helium and settle onto the EHB. The resulting total mass is only slightly larger than the helium-core mass, in contrast to normal main-sequence B stars whose masses are several times larger (Dorman et al., 1993; Heber, 2016).
The remaining envelope mass largely determines the position of the star on the EHB. A sufficiently thin hydrogen envelope produces the high effective temperatures and surface gravities characteristic of sdBs, while a more massive envelope results in cooler horizontal-branch stars. Evolutionary models generally require envelope masses below about $0.02\,M_\odot$, with canonical sdB models typically retaining only 10^{-3}–$10^{-2}\,M_\odot$ of hydrogen-rich material (Dorman et al., 1993; Han et al., 2002a).

The timing of envelope removal is crucial. If the envelope is stripped before the helium core has reached the required mass, the star may fail to ignite helium and instead evolve towards a helium white dwarf. Conversely, if the envelope is sufficiently removed after the core has become capable of helium ignition, the remnant can evolve onto the EHB and appear as an sdB (D'Cruz et al., 1996; Han et al., 2003). The observed properties of an sdB therefore retain information about the mass-loss process that produced it.

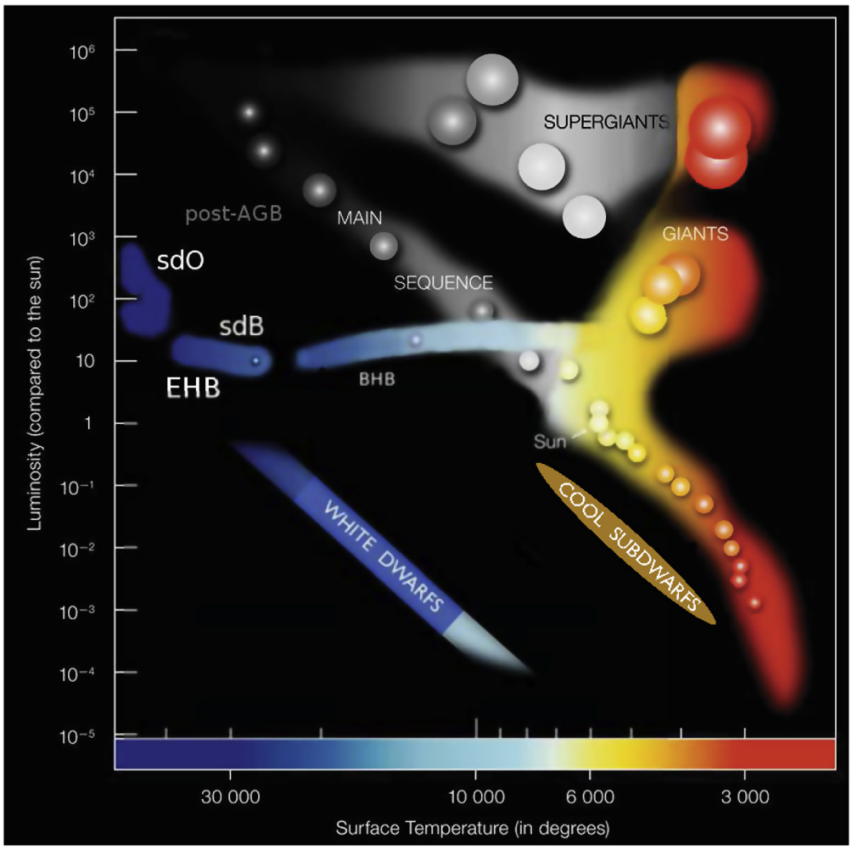


Figure 1.7: Location of hot subdwarf B stars on the extreme horizontal branch. Adapted from Heber (2009).

Figure 1.7 presents the location of sdB stars on the EHB. Their position reflects the combination of a helium burning core and a strongly reduced hydrogen envelope (Heber, 2009, 2016).

During the EHB phase, helium is converted into carbon and oxygen through the triple-α reaction and subsequent $^{12}\mathrm{C}(\alpha,\gamma)^{16}\mathrm{O}$ burning. Once central helium is exhausted, the star leaves the EHB and evolves towards the white dwarf cooling sequence. Because the hydrogen envelope is too thin to sustain the extended evolution of a normal asymptotic giant branch star, sdBs generally follow a post-EHB or AGB-manqué evolutionary path before becoming white dwarfs (Dorman et al.,

1993; Heber, 2009).

For a binary sdB, the properties of the stripped star are directly linked to the preceding binary interaction. Roche-lobe overflow or common envelope evolution can remove the hydrogen-rich envelope and determine the resulting sdB mass and orbital configuration. In the evolutionary pathway considered in this thesis, stable Roche-lobe overflow strips the initially more massive star to form the sdB, while the companion accretes mass and subsequently evolves towards a second interaction. The sdB is not an isolated endpoint of stellar evolution, but the product of the first stage of the binary evolutionary sequence investigated in this work (Ge et al., 2020; Han et al., 2003).

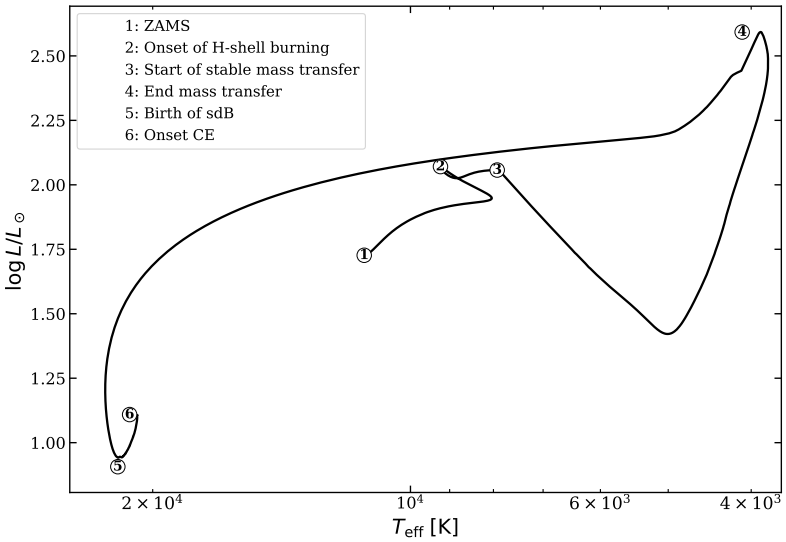


Figure 1.8: Evolutionary sequence of the binary system considered in this thesis, showing the formation of the sdB through stable Roche-lobe overflow and the subsequent common envelope phase.

Figure 1.7 places sdB stars in the broader context of stellar evolution. They occupy the hot end of the horizontal branch, at effective temperatures substantially higher than those of the red clump and cooler horizontal-branch stars. Their position on the EHB results from the strong reduction of the hydrogen-rich envelope while retaining a core massive enough to sustain helium burning. As the envelope becomes thinner, the star moves towards higher effective temperature and surface gravity, producing the compact configuration characteristic of sdBs. In the HR diagram, sdBs occupy a region distinct from both ordinary main-sequence B stars and the white dwarf cooling sequence even tough their temperatures can overlap with those of B-type stars, their luminosities and evolutionary states are different, while their ongoing core-helium burning distinguishes them from cooling white dwarfs (Dorman et al., 1993; Heber, 2009, 2016).

1.5.2 Formation channels

Hot subdwarf B stars can form through several evolutionary pathways, most of which involve the removal of the hydrogen-rich envelope of a red-giant progenitor. The main binary channels are common envelope (CE) ejection, stable Roche-lobe overflow (RLOF), and the merger of two helium white dwarfs (Han et al., 2003).

1. **common envelope ejection.**

   If mass transfer from a red-giant donor becomes dynamically unstable, the companion can become embedded in the donor's extended envelope. The resulting common envelope phase causes the binary components to spiral towards each other, transferring orbital energy and angular momentum to the envelope. If the envelope is successfully ejected, the exposed helium core can become an sdB star. The substantial reduction in orbital separation naturally produces compact post-CE binaries, including systems containing white dwarfs (Han et al., 2003; Ivanova et al., 2013).

2. **Stable Roche-lobe overflow.**

   If mass transfer remains stable, the donor can lose most of its hydrogen-rich envelope through prolonged RLOF without entering a common envelope. The stripped donor contracts towards the extreme horizontal branch and becomes an sdB star, while the companion can accrete part of the transferred material. Stable mass transfer can also widen the orbit and therefore generally produces wider sdB binaries than CE evolution (Chen et al., 2013; Ge et al., 2020; Han et al., 2003).

3. **Helium-white dwarf merger.**

   Two helium white dwarfs can lose orbital angular momentum through gravitational wave emission and eventually merge. If the merger remnant ignites helium, it can form a hot subdwarf. This channel generally produces a single sdB rather than a surviving binary (Hall and Jeffery, 2016; Han et al., 2003).

The observed binary population provides an important constraint on these formation channels. Close sdB binaries with orbital periods of hours to days are naturally associated with CE evolution, whereas wider systems are consistent with stable RLOF (Chen et al., 2013; Copperwheat et al., 2011; Han et al., 2003; Maxted et al., 2001; Napiwotzki et al., 2004; Vos et al., 2018). The coexistence of these populations indicates that more than one binary-interaction pathway contributes to the observed sdB population. Single-star mass loss and hot-flasher evolution can also produce

EHB stars, but these channels do not naturally produce the observed population of close sdB binaries (D'Cruz et al., 1996; Dorman et al., 1993; Heber, 2016).

1.5.3 Common envelope evolution

Common envelope evolution is crucial for compact binaries because it provides a mechanism for reducing an initially wider binary to the short orbital separations observed in systems such as sdB+WD binaries. Despite its importance, the physical process responsible for envelope ejection is not yet fully understood. Hydrodynamic calculations can follow the initial interaction and spiral-in, but connecting this dynamical phase to the complete ejection of the envelope remains challenging. Binary-evolution and population-synthesis calculations generally rely on parametrized prescriptions for the outcome of the CE phase (Ivanova et al., 2013).

The most widely used description is the energy formalism, which relates the binding energy of the donor's envelope to the change in orbital energy,

$$E_{\rm bind} = \alpha_{\rm CE} \left(E_{\rm orb,i} - E_{\rm orb,f} \right), \tag{1.20}$$

where $\alpha_{\rm CE}$ describes the efficiency with which the available orbital energy is used to eject the envelope. The envelope binding energy is commonly parametrized as

$$E_{\rm bind} = \frac{G M_d M_{\rm env}}{\lambda R_d}, \tag{1.21}$$

where M_d and $M_{\rm env}$ are the donor and envelope masses, R_d is the donor radius, and λ parametrizes the structure and binding of the envelope. Thus, λ describes the binding of the donor envelope, whereas $\alpha_{\rm CE}$ describes the efficiency of orbital-energy transfer into envelope ejection (Dewi and Tauris, 2000; Ivanova et al., 2013).

The simplicity of this prescription hides several uncertainties. The value of λ depends on the evolutionary state and internal structure of the donor, as well as on which contributions to the envelope binding energy are included. The calculations may consider only the gravitational binding energy or additionally include internal and recombination energy. The definition of the stellar core boundary also affects the inferred binding energy (Dewi and Tauris, 2000; Ivanova et al., 2013). Consequently, constraints on $\alpha_{\rm CE}$ cannot be interpreted independently of the assumptions used to determine $E_{\rm bind}$.

An alternative parametrization is the angular-momentum formalism, usually expressed through a parameter γ that relates the angular momentum carried away by the ejected material to the initial orbital angular momentum. While such pre-

scriptions can reproduce some observed post-CE systems, studies of white dwarf–main-sequence post-CE binaries have shown that the energy formalism provides a useful description of their observed orbital shrinkage (Zorotovic et al., 2010). These formalisms should be regarded as parametrizations of an incompletely understood physical process, not as unique descriptions of the CE phase, and the inferred efficiency is not necessarily universal across different donor populations (Ivanova et al., 2013; Zorotovic et al., 2010).

This issue is directly relevant to the evolutionary pathway considered in this thesis. In the sdb-first channel, the first interaction occurs through stable RLOF: the initially more massive primary loses its hydrogen-rich envelope and becomes the sdB, while the secondary accretes mass and is subsequently rejuvenated. The secondary later evolves into a giant and initiates a second interaction with the sdB. The resulting CE phase ejects the giant envelope and produces the compact sdB+WD system. The masses and orbital period of the final binary retain information about both the preceding stable mass-transfer episode and the efficiency of the subsequent CE phase.

Instead of adopting a universal value of $\alpha_{\rm CE}$, we reconstruct the CE evolution of the progenitors of compact sdB+WD systems and determine the efficiency required for each system to reach its observed post-CE configuration. The resulting $\alpha_{\rm CE}$ distribution can then be compared with constraints from other post-CE populations. This provides a test of whether the CE efficiency is consistent across different binary populations and evolutionary regimes.

Stable mass transfer is subject to a related set of uncertainties. Its outcome depends on the donor's response to mass loss, the binary mass ratio, the angular momentum carried away by non-accreted material, and the fraction of transferred mass retained by the accretor. This fraction is described by the mass-transfer efficiency β. In the evolutionary sequence considered here, β determines how strongly the secondary is rejuvenated during the first RLOF episode and therefore influences the mass and evolutionary state of the giant that later enters the CE phase. The initial masses, orbital period, and β determine the properties of the system entering the second interaction, while $\alpha_{\rm CE}$ governs the subsequent response during envelope ejection. For this reason, the stable-RLOF and CE phases are not independent in the evolutionary pathway studied here. The first interaction determines the structure and evolutionary state of the future CE donor, while the second interaction determines whether the resulting system can reproduce the observed compact sdB+WD configuration.

1.5.4 Evolution after core-helium burning

The sdB phase corresponds approximately to core-helium burning and typically lasts of order 10^8 yr. During this stage, helium is converted into carbon and oxygen in the core. Because the hydrogen envelope is very thin, the star does not normally undergo the extended giant evolution experienced by stars with more massive envelopes (Dorman et al., 1993; Heber, 2009).

After core-helium exhaustion, the star leaves the EHB and follows a post-EHB trajectory before eventually becoming a white dwarf. This evolution is often described as AGB-manqué or post-early-AGB evolution because the stripped star does not generally develop a normal thermally pulsing AGB phase (Dorman et al., 1993; Greggio and Renzini, 1990). Thus, the sdB represents a temporary stripped-core stage between red-giant evolution and the formation of a compact remnant.

In a binary system, the subsequent evolution is also determined by the companion. In the sdb-first pathway studied here, the companion has accreted mass during the first RLOF episode and therefore evolves subsequently on a modified timescale. It can eventually leave the main sequence, expand towards the giant branch, and interact with the sdB in a second phase of mass transfer. This later interaction is the common envelope phase that leads to the compact sdB+WD configuration relevant to the double-detonation progenitor scenario.

1.6 sdB+WD binaries

1.6.1 Formation of compact sdB+WD systems

The sdb-first pathway considered in this thesis produces the compact sdB+WD configuration through two successive phases of binary interaction. The first interaction strips the initially more massive star through stable Roche-lobe overflow, producing the sdB while transferring material to the secondary. The secondary is subsequently rejuvenated and evolves off the main sequence; when it expands as a giant, the second interaction can become dynamically unstable and lead to a common envelope phase. If the envelope is ejected, the system emerges as a compact sdB+CO WD binary.

This evolutionary sequence is distinct from the canonical WD-first scenario in which the WD forms before the sdB. In the sdb-first channel, the present-day masses, orbital period, and evolutionary states encode information about both mass-transfer episodes. The first episode determines the sdB core and envelope and the mass gained by the secondary, while the second interaction determines the WD mass

and the post-common envelope separation. This is why reconstructing the complete main-sequence history is necessary when interpreting an observed compact sdB+WD system.

1.6.2 Characteristic timescales

The evolutionary pathway considered in this thesis combines processes that operate on very different timescales. Distinguishing these timescales is important because the response of a star to mass loss depends on whether the mass-loss timescale is longer or shorter than the timescale on which the star can restore thermal or hydrostatic equilibrium. The nuclear, thermal, dynamical, and gravitational wave timescales therefore provide a physical framework for interpreting stable mass transfer, dynamically unstable mass transfer, and common envelope evolution (Ge et al., 2020; Hjellming and Webbink, 1987; Ivanova et al., 2013).

Nuclear timescale

The nuclear timescale estimates the duration over which nuclear burning can supply the stellar luminosity,

$$t_{\rm nuc} \sim \frac{E_{\rm nuc}}{L}.$$

For a main-sequence star, it is commonly approximated by

$$t_{\rm nuc} \sim \frac{\epsilon M c^2}{L},$$

where ϵ is the fraction of the stellar rest-mass energy available through nuclear burning. For low- and intermediate-mass stars, the main-sequence lifetime is typically 10^8–10^{10} yr, depending strongly on stellar mass and metallicity. The more massive stars in the grid therefore evolve more rapidly than solar-mass stars. If the donor remains in thermal equilibrium during Roche-lobe overflow, the mass-transfer rate may be driven by the nuclear expansion of the donor and proceed on the nuclear timescale (Ge et al., 2020; Hjellming and Webbink, 1987). The nuclear timescale thus determines when a component leaves the main sequence or reaches the giant branch and sets the timing of binary interaction.

Thermal timescale

The thermal, or Kelvin–Helmholtz, timescale is the time required for a star to radiate an amount of energy comparable to its gravitational binding energy:

$$t_{\rm th} \sim \frac{GM^2}{RL}.$$

When mass is removed rapidly enough to displace the donor from thermal equilibrium, but not rapidly enough to destroy hydrostatic equilibrium, the star readjusts on $t_{\rm th}$ and mass transfer proceeds on approximately the thermal timescale (Ge et al., 2020; Hjellming and Webbink, 1987). Stable Roche-lobe overflow from a radiative-envelope donor can therefore proceed on a thermal or nuclear timescale, depending on the mass-transfer rate and the evolutionary state of the donor. This distinction is central to the sdb-first channel because the first interaction must strip the primary's hydrogen-rich envelope while remaining dynamically stable (Ge et al., 2020; Han et al., 2002a).

Dynamical timescale

The dynamical timescale measures the response of a star to a loss of hydrostatic equilibrium:

$$t_{\rm dyn} \sim \left(\frac{R^3}{GM}\right)^{1/2}.$$

It is comparable to the free-fall or sound-crossing timescale and is typically of order hours for a normal star. If the donor's response to mass loss causes it to overflow its Roche lobe increasingly rapidly, mass transfer becomes dynamically unstable (Ge et al., 2010; Hjellming and Webbink, 1987). The resulting common envelope plunge-in is initiated on a dynamical timescale. However, the complete envelope-ejection process and the thermal relaxation of the remnant may extend beyond the initial plunge-in and remain uncertain (Ivanova et al., 2013). In this thesis, the common envelope phase is treated as a rapid orbital transition using the energy formalism rather than as a time-resolved hydrodynamical simulation.

gravitational wave timescale

After a compact binary has formed, gravitational wave radiation removes orbital energy and angular momentum. For a circular binary, the coalescence time in the

point-mass approximation is (Peters, 1964)

$$t_{\rm gw} = \frac{5}{256}\frac{c^5 a^4}{G^3 M_1 M_2 (M_1 + M_2)},$$

where a is the orbital separation. The corresponding local orbital-decay timescale is

$$\tau_{\rm gw} \equiv \frac{a}{|\dot{a}|} = \frac{5}{64}\frac{c^5 a^4}{G^3 M_1 M_2 (M_1 + M_2)}.$$

The factor-of-four difference reflects the distinction between the local decay timescale $a/|\dot{a}|$ and the integrated time to reach zero separation. For compact sdB+WD binaries, gravitational wave emission can drive the system into contact on a timescale of millions to hundreds of millions of years, depending strongly on the orbital period and component masses (Deshmukh et al., 2024; Geier et al., 2013; Peters, 1964).

1.6.3 Helium mass transfer and future evolution

Once the compact sdB+WD system has formed, gravitational wave emission continues to remove orbital energy and angular momentum. As the separation decreases, the Roche lobe of the sdB becomes progressively smaller until the donor can fill it and initiate Roche-lobe overflow onto the WD. Because the sdB has already lost most of its hydrogen-rich envelope, the transferred material is predominantly helium-rich. The subsequent mass-transfer rate, donor response, and WD accretion efficiency determine whether helium can accumulate in a sufficiently degenerate shell for ignition.

The observed systems CD-30°11223 and PTF1 J2238+7430 provide direct observational anchors for this evolutionary sequence. Their short orbital periods imply rapid gravitational wave-driven orbital evolution compared with wider sdB binaries, while their CO WD companions and helium-rich sdB donors make them physically relevant to the double-detonation channel.

Double-detonation models connect the sub-Chandrasekhar explosion mechanism directly to compact sdB+WD binaries, where helium-rich donors assemble the shells required to ignite the CO core. The formation of these systems is an essential part of the progenitor problem since, the explosion mechanism can be viable only if binary evolution can produce a CO WD and a helium-rich donor in a sufficiently compact configuration.

1.6.4 Known double-detonation progenitor candidates

Double-detonation progenitors require compact sdB+WD binaries in which gravitational wave-driven orbital decay eventually brings the sdB into contact, allowing helium to accumulate on the CO white dwarf. Two such systems have so far been identified as viable candidates. (Geier et al., 2013; Heber, 2009).

CD-30°11223

CD-30°11223 was the first hot-subdwarf + white dwarf binary to be identified as a double-detonation SN Ia progenitor candidate. Observations constrain the system to an ultra-compact orbit of $P_{\rm orb} \simeq 70.5\,\rm min$, with a hot subdwarf B star of $M_{\rm sdB} = 0.47^{+0.07}_{-0.06}\,M_\odot$ and a comparatively massive carbon–oxygen white dwarf of $M_{\rm WD} = 0.74 \pm 0.02\,M_\odot$ (Geier et al., 2013). gravitational wave radiation will drive the binary into contact on a timescale of $\sim 5 \times 10^7\,\rm yr$, initiating stable Roche-lobe overflow from the sdB onto the white dwarf. Recent analysis shows that this phase produces a helium shell of order 0.1–0.2 $M_\odot$ on the WD and that a shell detonation under these conditions robustly triggers a secondary core detonation, leading to a thermonuclear supernova (Deshmukh et al., 2024).

PTF1 J2238+7430

The recently identified system PTF1 J2238+7430 extends the sdB+WD double-detonation channel to lower sdB masses and slightly different orbital properties. Spectroscopic and photometric analyses show that it consists of a hot subdwarf B star of mass $M_{\rm sdB} = 0.41 \pm 0.02\,M_\odot$ and a white dwarf of $M_{\rm WD} = 0.72 \pm 0.03\,M_\odot$ in a $P_{\rm orb} = 76.34179\,\rm min$ orbit, making it one of the most compact sdB+WD binaries known. (Hernandez et al., 2026; Kupfer et al., 2022) use MESA to reconstruct the full evolutionary history of PTF1 J2238+7430 from the zero-age main sequence, showing that the sdB forms via a phase of stable Roche-lobe overflow from an $\sim 2.7\,M_\odot$ donor, followed by a common envelope phase that produces the present-day sdB+WD configuration. Their models demonstrate that gravitational wave-driven orbital decay will bring the sdB into contact, leading to a long-lived phase of helium mass transfer and the growth of a helium shell on the WD in the range required for a shell detonation to trigger a core detonation. They further describe the region of initial masses, orbital periods, and common envelope efficiencies that produce systems consistent with PTF1 J2238+7430.

1.7 Goal of the Thesis

The goal of this thesis is to answer the following questions:

- **What are the Main Sequence binaries that can evolve though the sdb-first channel and produce a binary like CD-30°11223?**
- **What is the range of common envelope efficiency that can reproduce CD-30°11223?**

Chapter 2

Methodology

2.1 Evolutionary Pathways for AM CVn

AM CVn are ultracompact, hydrogen-deficient interacting binaries with orbital periods in the range $P_{\rm orb} \sim 10$–$65\,{\rm min}$, typically consisting of a white dwarf accretor and a helium-rich donor (Solheim, 2010). Their short orbital periods make them strong source of gravitational waves, and their helium dominated spectra and secular evolution provide critical constraints on the mass transfer, common envelope evolution, and future evolution channel. Since, CD-30°11223 is expected to evolve into AM CVn before undergoing a double detonation explosion, It is natural to begin by reviewing the canonical AM CVn formation channels.

2.1.1 Classical Pathway

A comprehensive discussion of the proposed formation channels is given by Solheim (2010), who identifies three major channels:

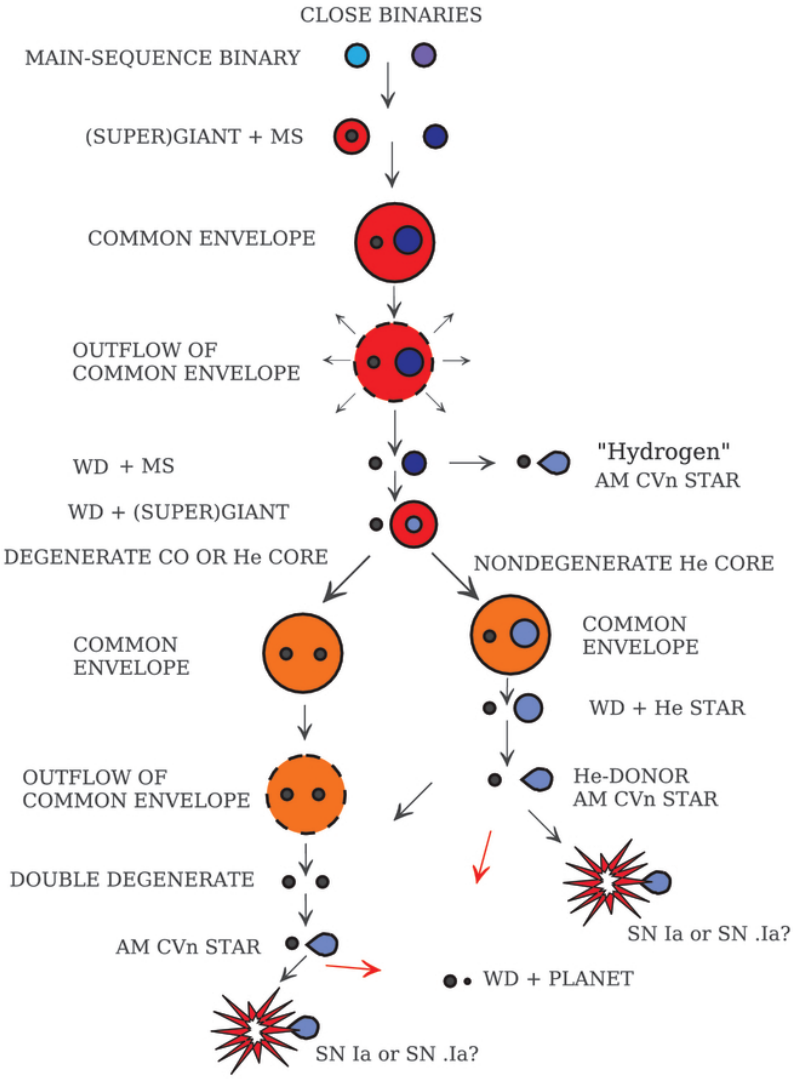


Figure 2.1: The Classical Evolution of AM CVn stars

1. **The double-degenerate white dwarf channel**: The progenitor is a close main-sequence binary in which the primary evolves first and fills its Roche lobe. This leads to dynamically unstable mass transfer and a common envelope phase, during which the hydrogen envelope of the red giant engulfs the secondary. The envelope is ejected, leaving a CO white dwarf with a non-degenerate companion. When the secondary later ascends the giant branch and again fills its Roche lobe, a second common envelope episode strips its hydrogen envelope. If the core of the secondary is not massive enough to ignite helium, the stripped remnant contracts and cools directly as a helium white dwarf. The post-CE system is thus a close CO WD + He WD binary, in which the accreting CO WD has formed first and the donor is already degenerate.

   gravitational wave radiation then shrinks the orbit until the He WD fills its

Roche lobe at an ultrashort period, initiating dynamically stable Roche-lobe overflow. The degenerate donor transfers helium to the CO WD at rates set by gravitational wave losses and its mass–radius relation, while the accretor builds up a helium shell whose properties depend on its mass and the accretion rate. For sufficiently massive CO WDs and helium shells, and accretion rates low enough to keep the shell strongly degenerate, the base of the helium layer can reach conditions for a thermonuclear runaway, triggering a helium shell detonation. In double-detonation models, the resulting shock compresses the CO core and induces a secondary detonation, producing a sub-Chandrasekhar Type Ia supernova.

2. **The helium-star channel** In this case after the first common envelope phase, the secondary is massive enough to ignite helium. It leads to form a He star + CO WD after the second common envelope phase. The orbit of the system reduces further via gravitational waves and leads to stable helium transfer to the primary. Under appropriate conditions (high accretor mass, sufficiently massive and degenerate helium shell, and moderate accretion rates), the base of this shell can reach the ignition threshold for a helium detonation, which can subsequently trigger a secondary detonation in the CO core in the double-detonation framework.

3. **The Hydrogen AM CVn channel** If the orbital separation after the first common envelope phase is too large to allow a second common envelope, the system evolves as a standard hydrogen-rich cataclysmic variable, consisting of a white dwarf accretor and a main-sequence donor in a wider orbit. In cases where the evolution is finely tuned such that a donor with mass of order $1.0\,M_{\odot}$ fills its Roche lobe when the central hydrogen abundance has already dropped below about 0.4, continued angular-momentum loss through magnetic braking and gravitational wave radiation can drive the system to shorter periods and strip the donor of most of its hydrogen envelope. The resulting binary then transitions from a hydrogen-rich CV to a long-period AM CVn star with a helium-dominated, semi-degenerate donor; this evolutionary pathway is referred to as the hydrogen-star channel (or evolved CV channel).

2.1.2 Alternate Pathway (sdB-First)

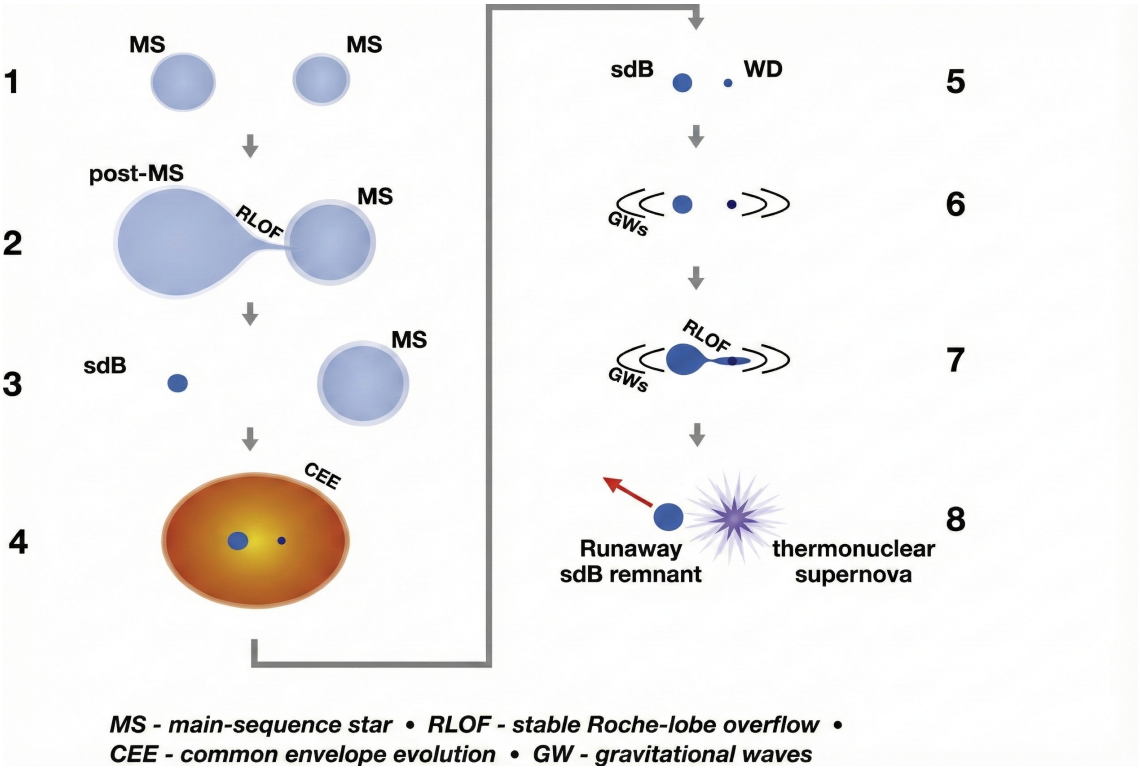


Figure 2.2: The Alternate Channel for AM CVn stars

The classical AM CVn formation pathway assumes that the CO white dwarf forms first during the initial common envelope phase, so that the accretor is always older than its companion. In this scenario, the pre-AM CVn system emerges as a detached CO WD + non-degenerate star, and a second common envelope phase later produces a compact CO WD + He WD binary in which the CO WD has already cooled for some time before the onset of mass transfer.

An alternative pathway, illustrated in Fig. 2.2, involves the formation of the sdb-first and requires only a single common envelope phase (Kupfer et al., 2022). In this channel, the initially more massive primary fills its Roche lobe while it still has a radiative envelope, leading to a phase of stable, largely conservative mass transfer. The primary is stripped of its hydrogen-rich envelope and becomes a core helium burning sdB, while the secondary accretes mass and becomes a more massive main-sequence star. The stable mass transfer widens the orbit. The now more massive secondary subsequently evolves off the main sequence, ascends the red-giant or asymptotic-giant branch, and fills its Roche lobe. Because of the extreme mass ratio and deep convective envelope, this second mass-transfer episode is dynamically un-

stable and drives a common envelope phase. Ejection of the envelope leaves behind a compact sdB+CO WD binary in which the sdB is older than the white dwarf and the orbital period has been reduced to tens of minutes.

After common envelope ejection, gravitational wave radiation extracts angular momentum from the sdB+WD binary, causing the orbit to shrink further. On a timescale set by the component masses and post-CE separation, the sdB fills its Roche lobe and initiates helium-rich mass transfer onto the CO WD. This sdB-first channel thus produces ultracompact sdB+WD systems that can evolve into AM CVn binaries and, for sufficiently massive accretors and appropriate mass-transfer rates, may reach the conditions required for helium shell ignition and a subsequent double-detonation Type Ia supernova.

2.1.3 Pathway for CD-30°11223

In particular, for CD-30°11223 the available observational and binary-evolution modeling indicates that the present hot subdwarf B star is a core helium burning EHB star with a mass of order $0.47\,M_{\odot}$, while its companion is a relatively massive CO white dwarf ($\gtrsim 0.74\,M_{\odot}$) in a $P_{\rm orb} \simeq 76\,$min orbit. These properties can be reproduced only in sequences where the sdB forms first, through a phase of stable, nearly conservative mass transfer from an initially more massive primary with a radiative envelope, and the current CO white dwarf is created later in a common envelope episode when the secondary ascends the giant branch (Deshmukh et al., 2024). The sdB is therefore the older component in CD-30°11223, in contrast to the classical AM CVn channels, which assume that the accreting white dwarf formed earlier and has already cooled before helium transfer begins.
Motivated by this constraint, we adopt the sdB-first alternate pathway as the evolutionary framework for CD-30°11223. Within this framework we focus on identifying viable progenitor configurations and quantifying how the key binary-evolution parameters, in particular the mass-transfer efficiency β and the common envelope efficiency $\alpha_{\rm CE}$, affect the formation of the observed sdB+CO WD system.

2.2 Modeling and Simulations

To model the binary evolution, we use the open-source stellar evolution code MESA (Modules for Experiments in Stellar Astrophysics) (version r24.08.1 of the MESA

code Paxton et al. 2011, 2013, 2015, 2018, 2019). MESA solves the coupled structure and composition equations for single and binary stars with adaptive mesh refinement and timestep control, and includes up-to-date microphysics such as equation-of-state tables, opacity routines, nuclear reaction networks, and prescriptions for mass loss and angular-momentum transport. Its binary module allows us to follow Roche-lobe overflow and wind mass loss in a self-consistent way, while specifying key parameters such as the mass-transfer efficiency β, initial system parameters, and boundary conditions. In the following subsections, we describe the specific MESA setups adopted for the alternate channel evolution of Main Sequence binary, including the initial progenitor configurations, the treatment of mass transfer and orbital evolution, and the choices of β explored in this work.

2.2.1 Simulation Setup

For our MESA simulations, the equation of state uses several sources, including OPAL (Rogers and Nayfonov, 2002), SCVH (Saumon et al., 1995), FreeEOS (Irwin, 2012), HELM (Timmes and Swesty, 2000), PC (Potekhin and Chabrier, 2010), and Skye (Jermyn et al., 2021). Nuclear reaction rates are adopted from a combination of the NACRE compilation (Angulo and et al., 1999), the JINA REACLIB database (Cyburt and et al., 2010), and tabulated weak reaction rates from Fuller et al. (1985), Oda and et al. (1994), and Langanke and Martínez-Pinedo (2000). Electron screening is treated following the prescription of Chugunov et al. (2007), while thermal neutrino energy losses are computed using the rates of Itoh and et al. (1996). Electron conduction opacities are taken from Cassisi et al. (2007), radiative opacities are primarily based on the OPAL opacity tables (Iglesias and Rogers, 1993, 1996), and Compton-scattering opacities at very high temperatures are calculated using the formalism of Buchler and Yueh (1976).
The binary evolution calculations were performed using the `binary` module of MESA. Mass transfer was treated using the Ritter prescription, allowing for stable Roche-lobe overflow. We adopted non-conservative mass transfer, parameterized by the mass-loss fraction β, where a fraction β of the transferred material is lost from the vicinity of the accretor while carrying its specific orbital angular momentum. The remaining angular momentum loss parameters associated with isotropic winds from the donor (α), circumbinary disks (δ), and additional systemic mass loss (γ) were set to zero. Angular momentum losses due to gravitational wave radiation, systemic mass loss, and spin–orbit coupling were included, whereas magnetic braking was neglected.

Tidal synchronization and circularization were enabled, with both stellar compo-

nents treated as rigid rotators. Wind mass loss and wind accretion were allowed for both stars, adopting a Bondi–Hoyle accretion efficiency of 1.5 and a maximum wind capture fraction of 1.0. Stellar models were evolved at solar metallicity ($Z = 0.02$) using an adaptively expanding nuclear reaction network.

Convective energy transport was treated using mixing-length theory with the Henyey formulation and a mixing-length parameter of $\alpha_{\mathrm{MLT}} = 2.0$. Convection was determined using the Ledoux criterion, with semiconvective mixing (efficiency = 1.0) and thermohaline mixing (coefficient = 2.0) included throughout the evolution. Predictive mixing was enabled following Ostrowski et al. (2021), together with rotationally induced instabilities, including the Solberg–Høiland instability, secular shear instability, Eddington–Sweet circulation, Goldreich–Schubert–Fricke instability, and the Spruit–Tayler dynamo (Heger et al., 2000, 2005). Convective core overshooting was modeled using the exponential prescription with $f = 0.016$ and $f_0 = 0.008$ for stars with masses exceeding $2, M_{\odot}$. Mass loss on the red giant branch and asymptotic giant branch was described using the prescriptions of Reimers (1975) ($\eta = 0.1$) and Blöcker (1995) ($\eta = 0.02$), respectively.

To ensure numerical stability during rapid evolutionary phases, particularly around helium ignition, restrictive timestep and convergence controls were adopted. Both stars were initialized with rotation rates equal to 1% of their critical values. The accretor was allowed to gain angular momentum during stable mass transfer and spin up accordingly. However, once the critical (breakup) rotation rate was reached, further spin-up was prevented, and stellar rotation was assumed to regulate the accretion rate following the prescription of Piersanti et al. (2003).

2.2.2 sdB formation through stable mass transfer

Both stars begin their evolution as detached, non-rotating main-sequence stars at the zero-age main sequence (ZAMS), with the primary set to be the more massive of the two. Stages 1 to 3 in Fig. 2.2 show how this initial configuration leads to the formation of the sdB. As the primary exhausts hydrogen in its core and moves through the subgiant branch, it expands and its envelope remains radiative rather than developing the deep convective envelope characteristic of a red giant (Stage 1). It is at this point, while the envelope is still radiative, that the primary is required to fill its Roche lobe. (Stage 2).

Whether this condition is met depends on the initial mass ratio of the binary. We therefore choose the initial masses of the two stars based on the adiabatic response of the donor to mass loss, which sets a critical mass ratio q_{crit} above which the donor cannot shrink its Roche lobe fast enough and mass transfer becomes dynamically

unstable. Stability is achieved when the initial mass ratio $q_{\rm init}$ is below this threshold. For conservative mass transfer from an intermediate-mass donor (1–6 $M_\odot$), $q_{\rm crit}$ evaluated at the end of the red giant branch (RGB) lies between 0.7 and 1 (Ge et al., 2020); restricting the grid to $q_{\rm init}$ below this range is what keeps the first mass-transfer episode in the stable regime required by this channel.

Once stable Roche-lobe overflow begins, the primary's hydrogen-rich envelope is steadily stripped while the secondary accretes the transferred material, growing more massive and, because angular momentum is carried outward with the transferred mass, widening the binary orbit as the mass transfer proceeds. Stripping continues until the primary is left with only a thin hydrogen layer (of order 10^{-3}–$10^{-2}\,M_\odot$) surrounding a helium core. As discussed in Chapter 1, if this core has already grown to the mass required for helium ignition (around 0.47 $M_\odot$) by the time stripping ends, the exposed core ignites helium and settles onto the extreme horizontal branch as an sdB star (Stage 3). The timing of the Roche-lobe overflow relative to the growth of the helium core is what decides the outcome, if envelope removal happens too early the core becomes sub-critical and the star instead contracts towards a helium white dwarf, while removal within the right window produces the core-helium burning sdB that this evolutionary channel requires. The secondary, now more massive and orbiting at a wider separation, carries on evolving towards the giant branch, setting up the second, dynamically unstable mass-transfer episode described in the next section.

2.2.3 White Dwarf formation through common envelope

After the stable mass transfer phase that forms the sdB star, the secondary continues its evolution with a more massive helium core. It leaves the main sequence, ascends the red giant branch, and ignites helium in its core. As the star expands, strong tidal interactions synchronize its rotation with the orbital motion, extracting orbital angular momentum and gradually shrinking the binary separation. Following core helium exhaustion, the secondary evolves toward the asymptotic giant branch, where its continued expansion causes it to fill its Roche lobe. This initiates a second phase of mass transfer, which rapidly becomes dynamically unstable, leading to a common envelope event. The envelope is subsequently ejected, leaving behind a proto-white dwarf that contracts and cools to form a carbon-oxygen white dwarf. Since MESA does not have the capabilities of simulating the hydrodynamics of the common envelope phase, we end the simulations just before the stage of common envelope (4 in fig 2.2) and numerically solve for the common envelope efficiency (α_{CE}).

To calculate the common envelope efficiency, we use the standard energy formalism of Webbink (1984).
We calculate the envelope energy (E_{bind}) by integrating the star envelope from the helium core boundary (i.e at radius where He mass fraction is 0.1) to the surface of the star,

$$E_{\rm bind} = -\int_{M_{\rm c}}^{M} \frac{Gm}{r(m)}\, dm + \int_{M_{\rm c}}^{M} \epsilon_{\rm int}(m)\, dm, \tag{2.1}$$

where the first integral represents the potential energy (E_{grav}), the second represents the internal energy (E_{int}), r is the radius, m is the mass, and ϵ_{int} is the specific thermodynamic internal energy.

We compute the initial orbital energy from

$$E_{\rm orb,i} = \frac{GM_{\rm c,1}M_{\rm c,2}}{2a_i}, \tag{2.2}$$

Here, $M_{c,1}$ is the CO core mass of the primary at the onset of envelope, $M_{c,2}$ is the total mass of the secondary, and a_i is the binary separation.

The final orbital energy is given by:

$$E_{\rm orb,f} = E_{\rm orb,i} - \frac{E_{\rm bind}}{\alpha_{\rm CE}}, \tag{2.3}$$

where, α_{CE} is the CE ejection efficiency. For each assumed α_{CE} between 0 and 1, we can calculate the corresponding final separation:

$$a_f = \frac{GM_{\rm c,1}M_{\rm c,2}}{2E_{\rm orb,f}}, \tag{2.4}$$

and derive the post-common envelope orbital period from Kepler's third law. This method allows us to map the final orbital configurations with pre and post common envelope parameters.

Chapter 3

MESA Grid and Analysis

3.1 Grid of Simulations

We simulated the Main-Sequence binaries through the alternate channel using the simulation setup described in 2.2.1. We created a grid of simulations by varying the 4 main-parameters:

Table 3.1: Parameter ranges explored in the MESA binary evolution grid.

Parameter	**Range**
$M_1,\ M_2\ (M_\odot)$	$1.8\ (1.0) - 6.8$
$q\ (M_2/M_1)$	$0.7 - 1.0$
$P_{\rm orb}$ (days)	$1.0 - 14.5$
β	$0.0 - 1.0$

- M_1 (primary mass) and M_2 (secondary mass; see Table 3.1): the initial component masses set the nuclear time-scales of the two stars and determine which star fills its Roche lobe first, as well as the core mass and structure at the onset of mass transfer. M_2 is chosen by varying M_1 with a step size of 0.2 $M_\odot$ in the given range and applying the constraint of mass-ratio (q). By varying M_1 and M_2, we sample progenitor mass combinations that can plausibly produce a core-helium burning sdB and a sufficiently massive CO white dwarf in a compact post-common envelope orbit, consistent with typical sdB progenitor masses and compact sdB+WD binaries discussed by Han et al. (2002a), Heber (2009), Geier et al. (2013), and Kupfer et al. (2022).

- $q = M_2/M_1$ (see Table 3.1): the initial mass ratio controls the stability and rate of Roche-lobe overflow, and thereby the nature of the first mass-transfer phase (stable versus dynamically unstable). Focusing on q close to unity allows us to identify combinations for which the initially more massive primary can undergo stable, nearly conservative mass transfer to form an sdB rather than entering a common envelope phase directly, in line with the stability criteria for sdB formation channels derived by Han et al. (2002a) and with detailed treatments of mass loss and envelope response in close binaries such as Ge et al. (2020).

- $P_{\rm orb}$ (initial orbital period; see Table 3.1): the starting orbital separation determines when each star fills its Roche lobe along its evolution (main sequence, subgiant, or giant branch), and thus whether mass transfer occurs under radiative or convective envelope conditions. Varying $P_{\rm orb}$ with a step size of 0.5 days within the specified interval enables us to map out which initial separations lead to the desired sequence of stable mass transfer from a radiative-envelope primary followed by a common envelope phase that produces a short-period sdB+CO WD binary, guided by the orbital-period ranges and interaction channels identified in sdB formation studies and compact sdB+WD systems (e.g. Geier et al., 2013; Han et al., 2002a; Kupfer et al., 2022).

- β (mass-transfer efficiency; see Table 3.1): the fraction of mass lost by the donor that is accreted by the companion directly affects the growth of the secondary, the response of the orbit to mass transfer, and the eventual mass of the CO WD. By varying β with step size of 0.1 from fully conservative to fully non-conservative, we probe how different accretion efficiencies influence the viability of sdB-first progenitors and the resulting sdB and white dwarf masses and separations, following the binary-evolution and Type Ia progenitor studies that treat β as a key free parameter (e.g. Hernandez et al., 2026).

Together, these parameters govern the mass budget, stability of mass transfer, and orbital evolution of the binary. Sampling a grid in $(M_1, M_2, q, P_{\rm orb}, \beta)$ therefore allows us to identify the regions of parameter space that can produce sdB + WD binaries and to quantify the sensitivity of the sdB-first formation channel to assumptions about the initial binary configuration and the efficiency of mass transfer.

To adequately cover this multidimensional parameter space, we constructed a discrete grid in $(M_1, M_2, q, P_{\rm orb}, \beta)$ as specified in Table 3.1. The chosen step sizes in

each dimension yield a total of **106,428** binary-evolution models, which we computed using MESA and ran in parallel on the *Hummel 2* high-performance computing cluster at Universität Hamburg. Each binary-evolution run typically required 4–5 hours of wall time; we executed the grid in parallel, using two CPU cores per model and up to 190 cores simultaneously, corresponding to an order of 10^5 core hours of total compute time.

3.2 Selection Procedure

The purpose of the grid is not simply to count how many binaries can form an sdB+WD system, but to determine which initial configurations allow the complete evolutionary sequence required by the sdB-first channel. The selection is therefore applied in stages that follow the physical sequence of the models: stable mass transfer must first occur, the primary must become a stripped helium burning star, the secondary must evolve towards a CO white dwarf, and the resulting compact binary must survive the interaction. This provides the connection between the large initial grid and the smaller population whose properties can be meaningfully compared with observed compact sdB+WD systems.

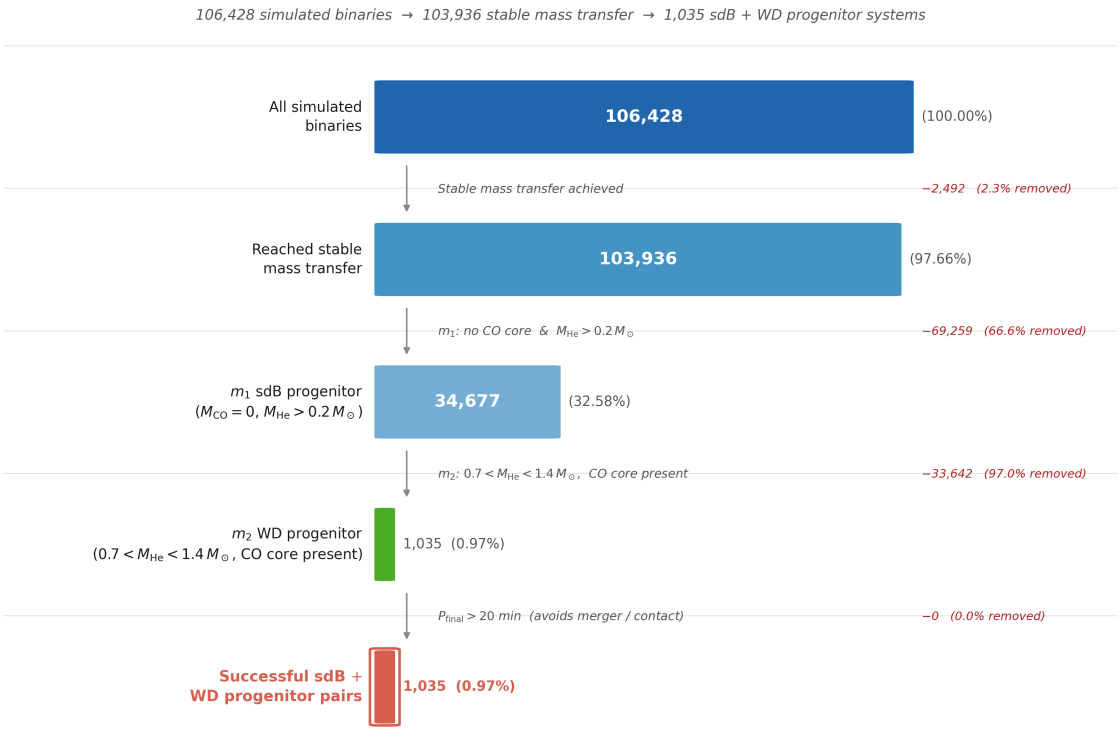


Figure 3.1: Selection Procedure

The full grid contains 106,428 simulated binaries. Of these, 103,936 reach stable mass transfer – only a small fraction is removed at this first stage. Requiring the primary to become an sdB progenitor (no CO core, and a helium core mass above $0.2\,M_{\odot}$) is a much harder cut: it brings the sample down to 34,677 systems. A further requirement is imposed on the companion, which must retain a CO core and have a helium core mass in the range $0.7\,M_{\odot} < M_{\rm He} < 1.4\,M_{\odot}$, leaving 1,035 sdB+WD progenitor systems. Finally, we exclude systems that would merge or enter contact, requiring a final orbital period of $P_{\rm final} > 20$ min; every one of the 1,035 selected systems already satisfies this condition. The full selection procedure therefore reduces the original grid to 1,035 successful sdB+WD progenitor pairs.

3.3 Successful Candidates/Systems

The selection procedure leaves **1,035 systems** that complete the required evolutionary sequence and form an sdB+WD binary. We now use this population to determine preferred region of the initial parameter space. Establishing this first is important because it shows which combinations of initial masses and orbital periods are capable of producing the channel at all, before applying the more restrictive constraints from a particular observed system.

3.3.1 2D Histogram of Period vs Primary Mass

The first property to examine is the location of the successful systems in the initial mass–period plane. These two quantities set the evolutionary timescales of the stars and determine when the primary fills its Roche lobe, so their distribution provides a direct view of the initial configurations from which the sdB-first sequence can arise.

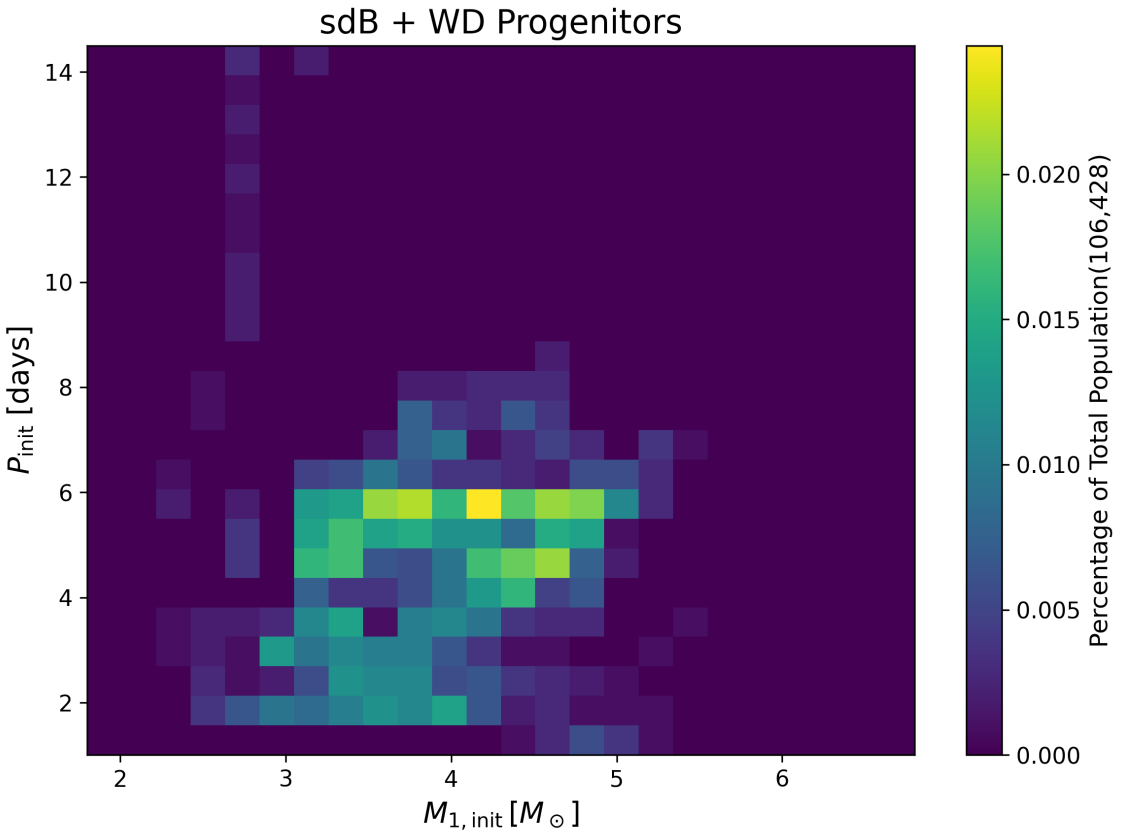


Figure 3.2: 2D Histogram for period vs primary mass

Figure 3.2 shows the two-dimensional histogram of the initial primary mass ($M_{1,\text{init}}$) and orbital period (P_{init}) for systems that successfully evolve into an sdB + WD binary. The color scale gives the percentage of the total simulated population, so it maps out the relative formation efficiency across the parameter space directly. The successful progenitors are concentrated within a relatively narrow region, favouring intermediate-mass primaries ($3 \lesssim M_{1,\text{init}} \lesssim 5\,M_\odot$) and initial orbital periods of approximately $2 - 8$ days, with the highest density of successful systems occurring near $M_{1,\text{init}} \approx 4\,M_\odot$ and $P_{\text{init}} \approx 5 - 6$ days.

Outside this region the number of successful systems falls off sharply, so the formation of sdB + WD binaries clearly needs a well-defined range of initial conditions. Systems with shorter orbital periods tend to initiate Roche-lobe overflow too early, often resulting in unstable mass transfer or merger events, while wider binaries interact too late to efficiently strip the primary star and produce an sdB star. Likewise, primaries with masses below or above the preferred range follow different evolutionary pathways, which lowers the odds of forming an sdB + WD system. Even though some variation in the initial parameters is tolerated, the fact that the high-density region stays this compact shows how sensitive the outcome is to the initial binary

configuration.

3.3.2 Initial Mass Space

The previous distribution describes the successful population in terms of two initial quantities. To understand the binary configuration more completely, we next examine the initial component masses and mass ratio. The mass ratio is important because the first interaction must remain stable long enough to strip the primary and form the sdB. The following distributions therefore test whether the concentration seen in the period–mass plane is accompanied by a preferred mass ratio.

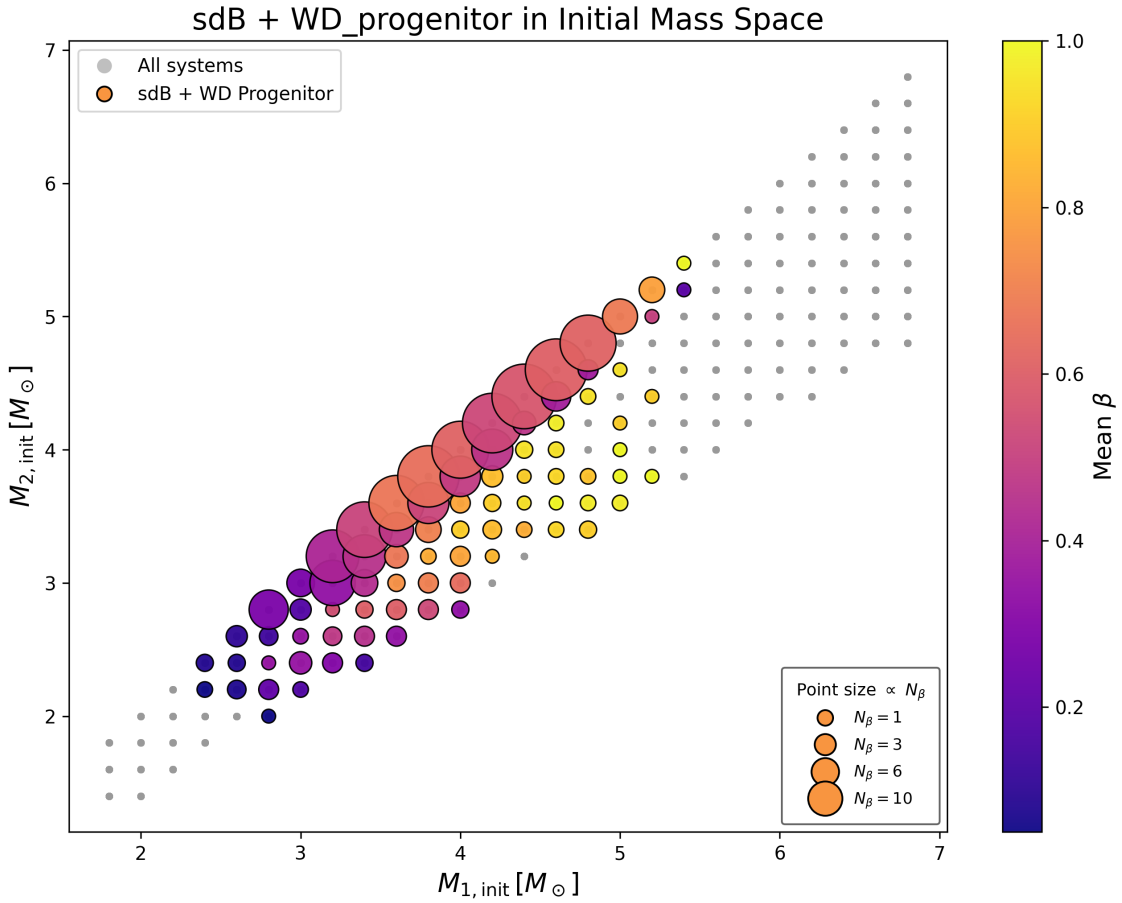


Figure 3.3: Mass Space of successful systems

Figure 3.3 shows the distribution of the initial binary masses for all simulated systems and for those that successfully evolve into an sdB + WD binary. The gray points represent the complete grid of 106,428 simulated binaries, while the coloured points correspond to successful progenitors. The colour indicates the mean mass transfer efficiency, β, and the marker size is proportional to the number of successful systems sharing the same initial mass combination but differing in the initial

orbital period or β.

The successful progenitors occupy only a limited region of the available parameter space as the formation of sdB + WD systems clearly needs a fairly narrow range of initial stellar masses. The largest markers sit along the diagonal corresponding to mass ratios close to unity ($q = M_{2,\mathrm{init}}/M_{1,\mathrm{init}} \approx 1$) binaries with nearly equal-mass most likely successful because they are the ones that experience stable Roche-lobe overflow, letting the primary envelope be stripped efficiently without triggering a premature common envelope phase.

There is also a systematic trend in the mass-transfer efficiency. Lower-mass progenitors preferentially evolve through solutions with smaller values of β, while binaries with more massive primaries favour progressively larger β. In other words, systems with higher-mass donors need to lose a greater fraction of the transferred material from the binary altogether in order to keep the mass transfer stable and still end up with the observed sdB + WD configuration.

The growing spread in $M_{2,\mathrm{init}}$ towards higher $M_{1,\mathrm{init}}$ simply follows from how the grid was sampled. As the primary mass increases, more secondary masses satisfy the allowed mass-ratio criterion, so the distribution naturally broadens. Even so, with this larger parameter space available, the successful progenitors still cluster around mass ratios close to unity.

3.3.3 Parameters Distribution

The distributions of the individual parameters provide a more quantitative description of the successful region identified above. They allow us to distinguish broad properties of the channel from the correlations between parameters and to establish the initial conditions that are most frequently associated with successful sdB+WD formation.

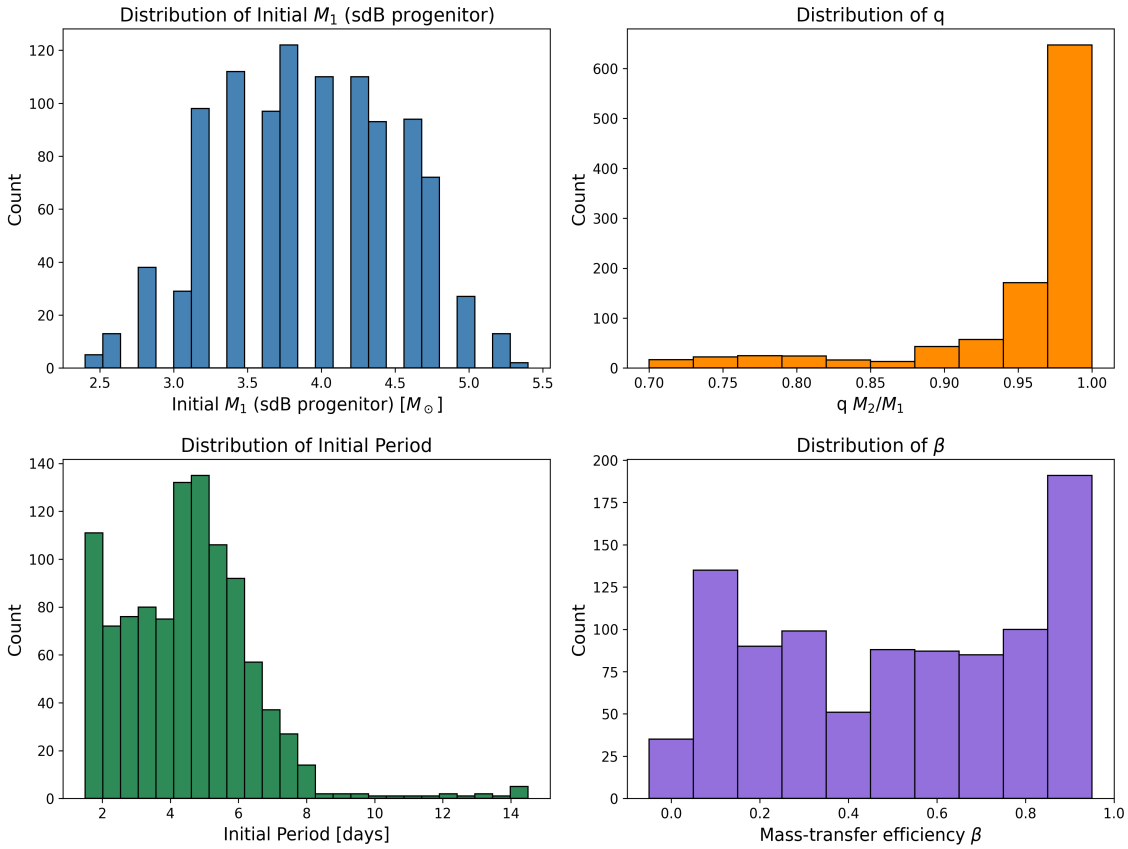


Figure 3.4: Parameter Distribution

Figure 3.4 presents the distributions of the initial binary parameters for the 1,035 systems that successfully evolve into an sdB + WD binary. The four panels summarize the distributions of the initial primary mass, the initial mass ratio, the orbital period, and the mass-transfer efficiency (β), highlighting the preferred regions of parameter space that yield successful progenitors.

- The initial primary mass spans roughly $2.5 - 5.5\,M_\odot$, with most successful systems clustered between 3.2 and $4.8\,M_\odot$, consistent with the two-dimensional analysis above. Intermediate-mass primaries are simply the ones that give the most favorable conditions for stable envelope stripping and sdB formation.

- The initial mass ratio has a spread over the range of the input values but peaks sharply near $q \approx 1$ i.e. binaries with nearly equal-mass components are strongly preferred, because they are the ones most able to undergo stable Roche-lobe overflow, removing the primary envelope efficiently instead of tipping into dynamically unstable mass transfer.

- The initial orbital period is concentrated between roughly 2 and 6 days, peaking near $4 - 5$ days. A handful of successful systems reach longer periods,

but their numbers drop off quickly showing only a narrow range of orbital separations gives the right conditions for stable binary interaction.

- The mass-transfer efficiency, by contrast, is broadly distributed over nearly the full range of β, though successful progenitors skew towards higher values and keeping only a small fraction of the transferred mass appears to be enough to reproduce the observed sdB + WD systems. That breadth is itself informative because it means the required mass-transfer efficiency is not fixed, but depends on the rest of the initial binary configuration.

Chapter 4

CD-30 Progenitors

The previous chapter established the population of binaries that can complete the sdB-first evolutionary sequence. The remaining question is how many of these systems can reproduce the properties of an observed compact sdB+WD double-detonation candidate, since the models now have to match not just the right evolutionary sequence but also the present-day component masses and orbital configuration of the real system. This chapter narrows the general successful population down to the subset that can reproduce CD-30°11223 in two stages: first by checking which systems fall within the observed component masses, and then by matching each system's post-common envelope orbital period against the value reconstructed from the present-day orbit.

4.1 sdB and WD Mass Constraints

The most direct observed constraints on CD-30°11223 are the present-day masses of its two components. Figure 4.1 compares these against the mass distributions of the full successful progenitor population, as a first check of how many of the 1,035 systems are even in the right mass range.

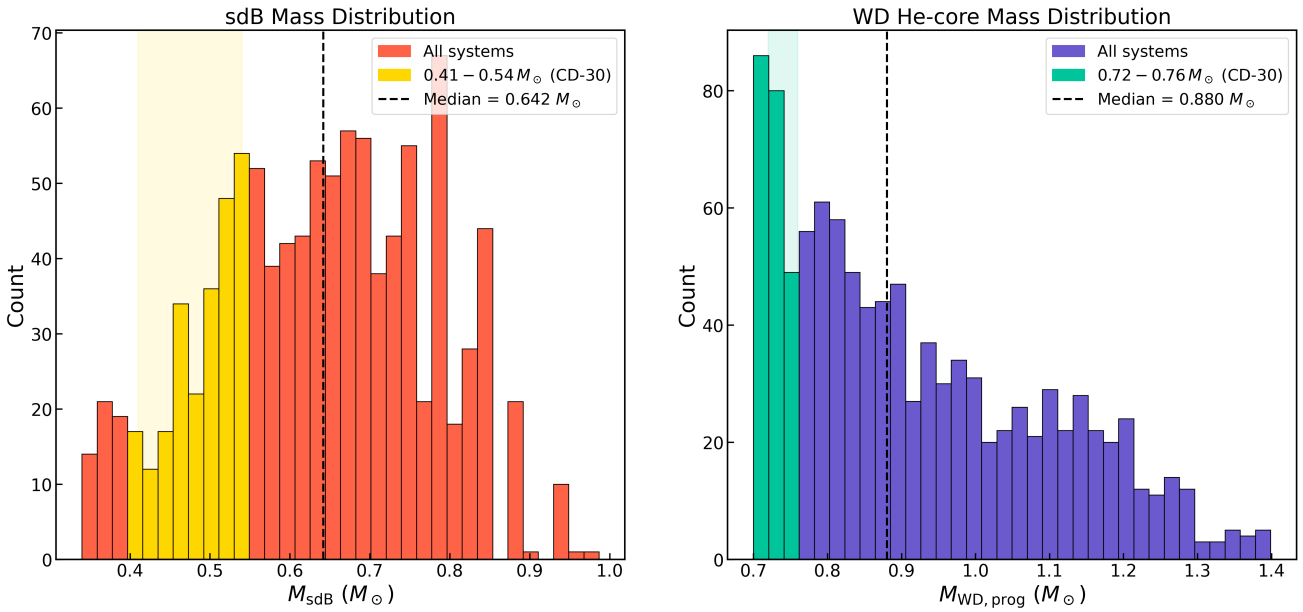


Figure 4.1: sdB and WD mass distribution

Figure 4.1 compares the final mass distributions of the sdB star and its white dwarf companion for all successful sdB + WD progenitors with the subset of systems satisfying the observed mass constraints of CD-30°11223. The coloured histograms represent the complete population of successful progenitors, while the highlighted regions correspond to systems within observed mass ranges of $0.41 - 0.54\,M_\odot$ for the sdB star and $0.72 - 0.76\,M_\odot$ for the white dwarf companion. The dashed vertical lines indicate the median masses of the complete progenitor population.

The sdB mass distribution spans a broad range from approximately 0.35 to $0.98\,M_\odot$, with a median value of $0.642\,M_\odot$. The observational constraint for CD-30°11223 only selects the low-mass tail of this distribution, since the observed sdB is noticeably lighter than the sdB a typical simulated system produces. Only a comparatively small fraction of successful sdB + WD systems actually match the measured sdB mass.

The white dwarf progenitor mass tells a similar story. The successful population covers helium-core masses from about 0.76 to $1.40\,M_\odot$, with a median of $0.880\,M_\odot$. The observed white dwarf mass of CD-30°11223 ($0.72 - 0.76\,M_\odot$) sits near the lower edge of that range, again picking out only a small subset. Matching both masses simulataneously is a stronger constraint but still mass alone is fairly loose. Both windows are broad, and a system can sit inside them without actually reproducing the system's orbital configuration. The next step applies a tighter, more direct filter by matching each progenitor's predicted post-common envelope orbital period against the value reconstructed from CD-30°11223's present-day orbit. This

identifies the specific progenitor candidates that have the mass as well as orbital parameters matching the observed values.

4.2 Identification of CD-30°11223 Progenitor Systems

The 1,035 successful systems identified in the previous chapter form the parent population for the CD-30°11223 analysis. The present orbital period, though, cannot be compared directly with the separation right after the common envelope phase, since the system has kept evolving through gravitational wave emission since the envelope was ejected. We therefore first need to reconstruct the post-CE orbital period the observed system must have had, so that we have a quantity we can actually compare against each progenitor model's CE outcome.

After the CE ejection, the subsequent orbital evolution is assumed to be governed solely by the emission of gravitational waves. By integrating the orbital decay equations derived by Peters (1964), the orbital period immediately after the CE phase is given by

$$P_{\mathrm{CE,cool}} = \left[P_{\mathrm{obs}}^{8/3} + \frac{256}{5} \frac{G^{5/3}}{c^5} (2\pi)^{8/3} \frac{M_1 M_2}{(M_1 + M_2)^{1/3}} t_{\mathrm{cool}} \right]^{3/8}, \tag{4.1}$$

where P_{obs} is the observed orbital period, M_1 and M_2 are the masses of the white dwarf and sdB star, respectively, and t_{cool} is the white dwarf cooling age.

Using the observed parameters of CD-30°11223 (Deshmukh et al., 2024; Geier et al., 2013), namely $M_1 = 0.47\,M_\odot$, $M_2 = 0.74\,M_\odot$, $P_{\mathrm{obs}} = 70.53\,\mathrm{min}$, and $t_{\mathrm{cool}} = 39\,\mathrm{Myr}$, we obtain a reconstructed post-common envelope orbital period of

$$P_{\mathrm{CE,cool}} = 88.7\,\mathrm{min}.$$

For each binary model, the post-common envelope orbital separation, a_{f}, was calculated using the common envelope energy formalism (Equation 2.4). The corresponding post-common envelope orbital period was then determined from Kepler's third law,

$$P_{\mathrm{CE,model}} = 2\pi\sqrt{\frac{a_{\mathrm{f}}^3}{G\,(M_1 + M_2)}}, \tag{4.2}$$

where a_{f} is the orbital separation immediately after the CE phase.

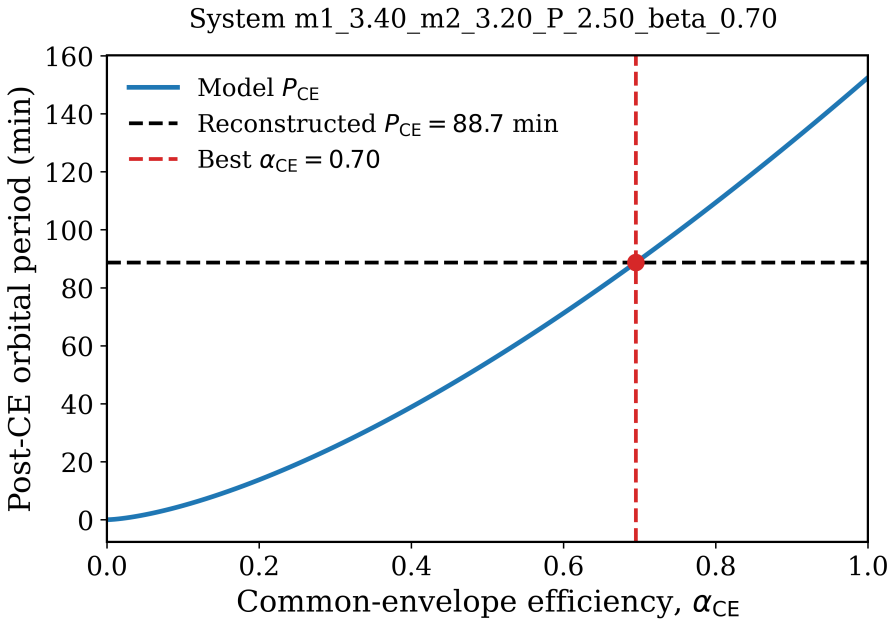


Figure 4.2: Example of the progenitor selection procedure for a representative binary model. The blue curve shows the post-common envelope orbital period predicted by the model as a function of the common envelope efficiency parameter, α_{CE}. The horizontal dashed line represents the reconstructed post-common envelope orbital period of CD-30°11223 ($P_{\mathrm{CE,cool}} = 88.7\,\mathrm{min}$), while the vertical dashed line indicates the value of α_{CE} that provides the closest match. This procedure was repeated for every simulated binary to identify viable progenitor systems of CD-30°11223.

The above calculation was repeated over the full range of assumed common envelope efficiencies, α_{CE}. For each model, the value of α_{CE} that produced a post-common envelope orbital period closest to the reconstructed value of $P_{\mathrm{CE,cool}} = 88.7\,\mathrm{min}$ was identified. There were total **53 systems** that satisfied this criterion and hence were selected as viable progenitor candidates for CD-30°11223 and were subsequently used in the analysis presented in the following sections.

4.3 Mass Space of Candidates

To investigate the range of initial binary configurations that can give rise to the observed properties of CD−30, we first examine the distribution of the initial masses of the progenitor systems. The initial masses of the two stars are important parameters in determining their subsequent binary evolution, as they influence the mass transfer history, the evolutionary timescales, and the final properties of the white dwarf–hot subdwarf system.

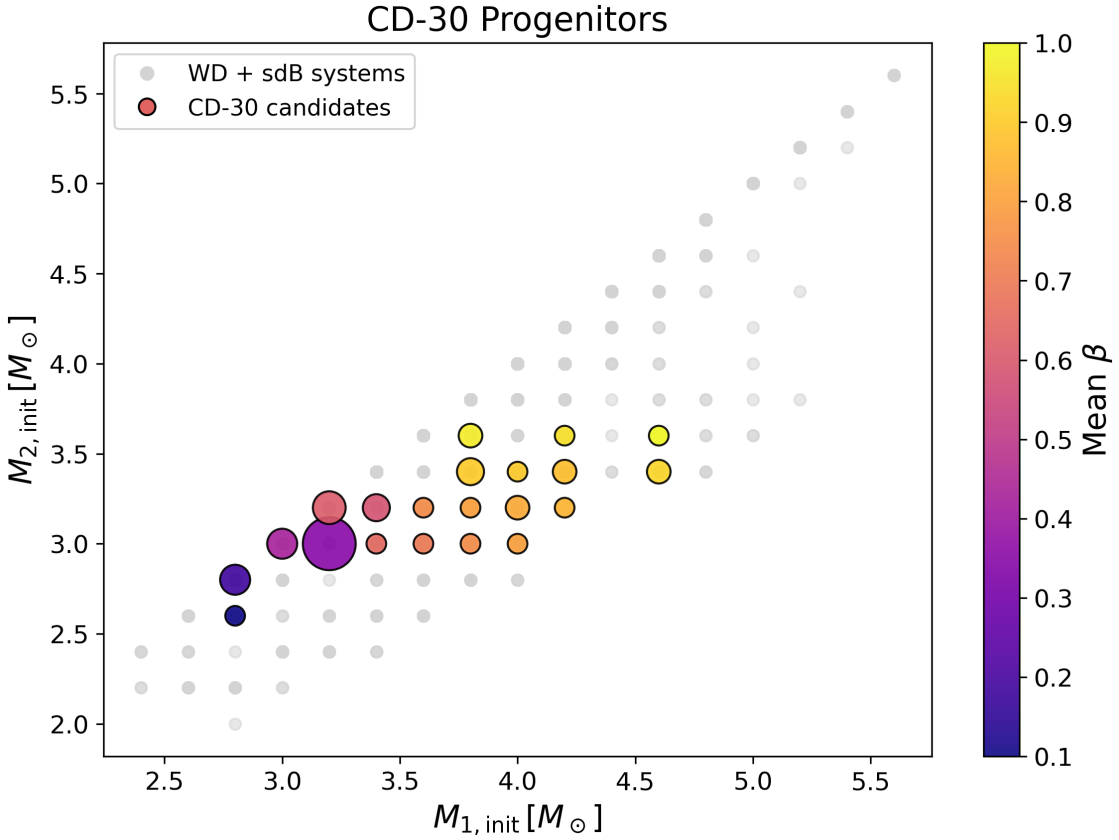


Figure 4.3: Mass Space of the possible progenitors of CD-30

The grey points represent all successful WD+sdB systems in the explored parameter space, while the colored circles indicate the identified CD−30 progenitor candidates. The color of each circle corresponds to the mean mass-transfer efficiency parameter (β) of the successful models associated with a given initial mass pair. The size of each circle is proportional to the number of successful models for a particular combination of $M_{1,\mathrm{init}}$ and $M_{2,\mathrm{init}}$, including models with different values of β and initial orbital period. The distribution of the colored points therefore illustrates not only the range of initial masses capable of producing a CD−30-like system, but also how the successful solutions are distributed within the explored parameter space.

Within the explored parameter space ($0.7 \leq q_{\rm init} \leq 1.0$), the successful CD$-$30 progenitors preferentially occupy the high-mass-ratio regime, with a median value of $q_{\rm init} = 0.938$ and a standard deviation of $\sigma_q = 0.079$. This indicates that progenitors with nearly equal initial stellar masses are favored among the successful models. To examine the relationship between the initial mass ratio and the mass-transfer efficiency, we use the Spearman rank correlation coefficient (Spearman, 1904),

$$r_{\rm S} = 1 - \frac{6 \sum_i d_i^2}{n(n^2 - 1)}, \tag{4.3}$$

where d_i is the difference between the ranks of the i-th pair of $q_{\rm init}$ and β values, and n is the number of progenitor systems. We find a Spearman rank correlation coefficient of $r_{\rm S} = -0.557$, indicating a moderately strong inverse relationship between $q_{\rm init}$ and β. The corresponding p-value is $p = 4.4 \times 10^{-6}$, indicating that the observed anti-correlation is statistically significant. In practical terms, systems with lower initial mass ratios tend to require higher β to reproduce the observed properties of CD$-$30. This suggests that the initial mass ratio and the mass-transfer efficiency are linked in determining the evolutionary pathways leading to the observed white dwarf–hot subdwarf configuration.

4.4 Distributions of CD-30 progenitors

The mass-space plot identifies where the viable progenitors lie, but it does not show how sharply the individual initial parameters are constrained. We therefore examine their one-dimensional distributions together. This allows the preferred primary mass, mass ratio, initial period, and the two efficiency parameters to be considered as parts of the same progenitor population rather than as independent results.

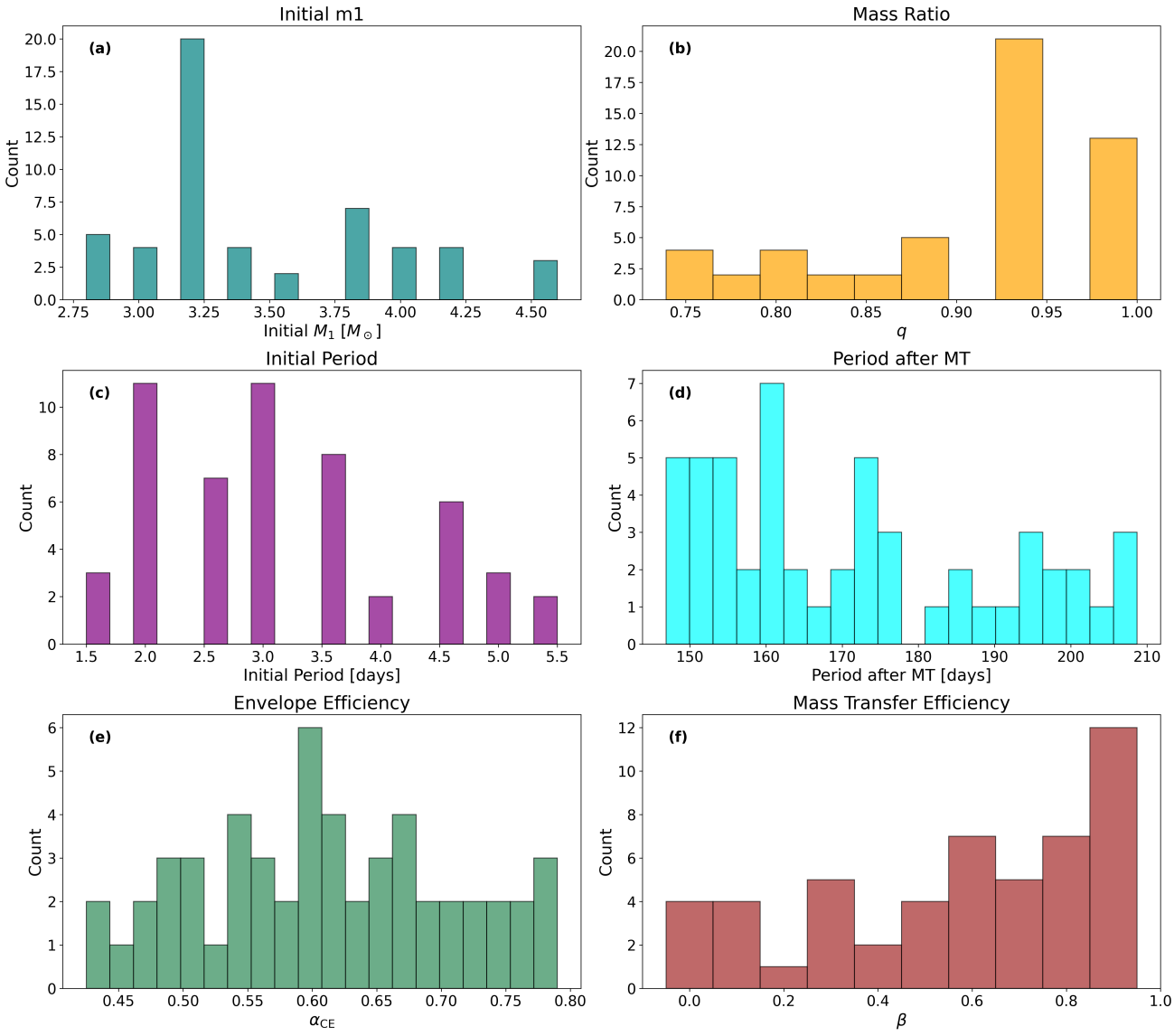


Figure 4.4: Parameter distribution of CD-30 progenitors

- **Panel (a)** The successful CD−30 progenitors are concentrated in the range $M_{1,\mathrm{init}} \simeq 2.8$–$5.2\,M_\odot$, despite the model grid extending from 1.8 to $7.0\,M_\odot$. They cluster around $M_{1,\mathrm{init}} \sim 3.2\,M_\odot$, which is where the conditions are best for the sequence of stable mass transfer and common envelope evolution this formation channel requires.

- **Panel (b)** High initial mass ratios dominate, with most systems clustered around $q \simeq 0.9$–1.0. Binaries with comparable component masses are the ones most able to undergo stable Roche-lobe overflow during the first mass-transfer phase, whereas lower mass ratios are more prone to unstable mass transfer as discussed in chapter 2 & 3. Nearly equal mass binaries keep the mass exchange stable while still letting the future sdB progenitor grow enough.

- **Panel (c)** Successful progenitors also favour short initial orbital periods ($\sim$ 1.5–3.5 days), which points to the timing of the first Roche-lobe overflow as a key factor. Early mass transfer strips the hydrogen-rich envelope before the core grows too much, producing a stripped helium burning star with masses in the range $\sim$ 0.40–0.52 $M_{\odot}$. Wider binaries, by contrast, transfer mass at more advanced evolutionary stages and end up with different core masses and outcomes altogether. So the preference for short-period progenitors ties the formation of CD$-$30 directly to early envelope stripping and the helium-core mass set at the onset of binary interaction.

- **Panel (d)** After the stable mass-transfer phase, the successful progenitors settle into a fairly narrow range of orbital periods, mostly between $\sim$ 150 and 210 days. That is just the orbital expansion expected when the initially more massive donor transfers mass to its companion, and it means only a limited set of post-mass-transfer configurations can go on to evolve through a common envelope phase into a CD$-$30-like system.

- **Panels (e) and (f)** show the distributions of the common envelope efficiency ($\alpha_{\rm CE}$) and the mass-transfer efficiency (β) for the successful progenitors. The values of $\alpha_{\rm CE}$ span a range of $\sim$ 0.43–0.79, with a mild concentration around $\alpha_{\rm CE} \sim 0.6$. In contrast, the distribution of β is skewed towards higher values, with most successful progenitors having $\beta \gtrsim 0.5$ and a substantial fraction concentrated between $\beta \sim 0.8$ and 1.0. This indicates that the successful progenitors generally favour non conservative mass transfer, while the common envelope phase can produce successful systems over a broader range of efficiency values.

4.5 Initial Period vs β

The preceding distributions show that the viable systems favour particular initial periods and mass-transfer efficiencies, but they do not by themselves show how these quantities are coupled to the CE phase. Because β determines how much of the transferred mass is retained by the secondary and therefore changes the mass and evolutionary state of the star that later enters the CE, its effect must be considered together with the initial period and $\alpha_{\rm CE}$. The following figure examines this connection directly.

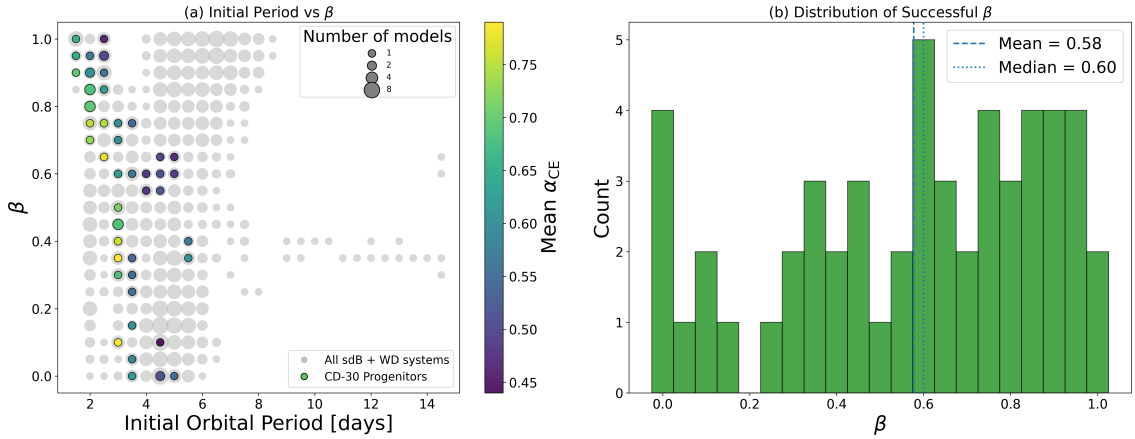


Figure 4.5: Initial Period and β distribution of the candidates as a function of α & β

The successful progenitors span the full range of mass-transfer efficiencies from fully conservative ($\beta = 0$) to fully non-conservative ($\beta = 1$). The distribution is weighted towards higher values, with a mean of $\langle\beta\rangle = 0.58$, a median of $\beta = 0.60$, and an interquartile range of 0.35 to 0.85. Approximately 57% of the systems have $\beta \geq 0.60$, while $\geq 35\%$ have $\beta \geq 0.75$, indicating that relatively non-conservative mass transfer is common among the successful progenitors.

The left panel further shows a dependence of β and $\alpha_{\rm CE}$ on the initial orbital period. Systems with short initial periods ($P_{\rm init} \lesssim 3\,{\rm d}$) preferentially exhibit higher β and lower $\alpha_{\rm CE}$, whereas systems with longer initial periods span a broader range of β values. This suggests that compact progenitors generally require greater mass and angular-momentum loss during the early stages of binary evolution to reach the observed orbital configuration. The presence of successful systems across the full range of β nevertheless indicates that CD$-$30 like systems are not restricted to a unique mass-transfer prescription.

4.6 sdB and WD Evolution

The dependence on β has a physical consequence that is important for the second interaction. The secondary is the star that later becomes the CE donor, so its mass and evolutionary state after the first mass-transfer episode determine the conditions under which the CE begins. We therefore next follow how the first interaction changes both components and the orbital configuration of the viable progenitors.

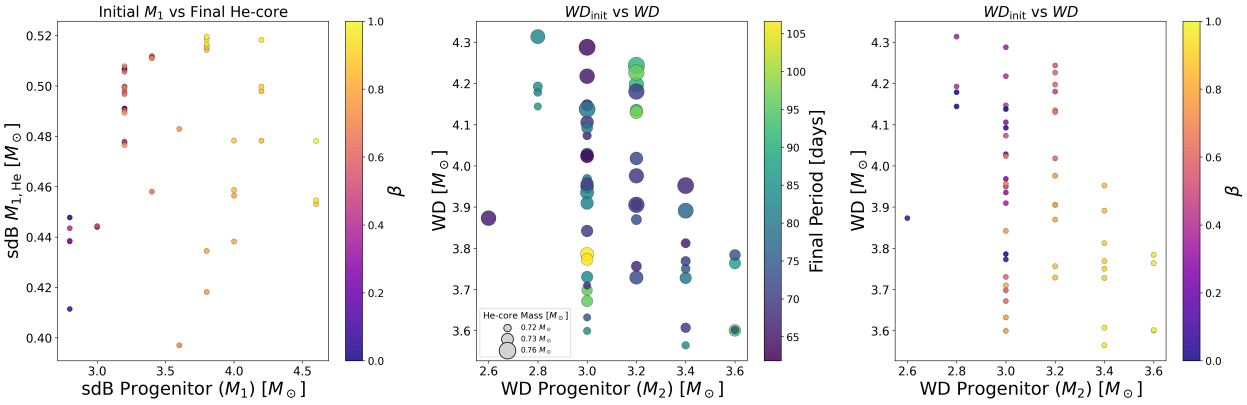


Figure 4.6: M2 and M1 evolution for the candidates as a function of β

- The left panel plots the final helium-core mass of the donor (the future sdB star) against its initial mass, coloured by the mass-transfer efficiency β. Successful progenitors span a fairly broad range of initial donor masses ($M_{1,\mathrm{init}} \simeq 2.8$–$4.6\,M_\odot$), yet the resulting helium-core masses stay packed into a much narrower band, $M_{1,\mathrm{He}} \simeq 0.40$–$0.52\,M_\odot$. In other words, the first Roche-lobe overflow has to happen within a fairly tight evolutionary window to give sdB stars with similar core masses, even when the initial donor masses differ quite a bit. There is no strong correlation between β and the final sdB mass here, so the donor core mass looks like it is set mainly by how evolved the star already is when mass transfer begins and not by efficient mass transfer.

- The middle and right panels follow the accretor through the stable mass-transfer phase. Post-transfer masses are in the range $M_{2,\mathrm{after\,MT}} \simeq 3.6$–$4.3\,M_\odot$, substantial growth from the initial secondary mass. In the middle panel, colour marks the final orbital period and marker size the accretor's final helium-core mass; systems with larger helium cores tend to sit lower on the diagram because initially more massive accretors are further along in their own evolution. Final orbital periods span roughly 60–105 days, so quite a range of post-mass transfer configurations can still go on to become CD-30 like systems. The right panel, coloured by β, makes the dependence on mass-transfer efficiency explicit: lower β (more conservative transfer) builds more massive accretors, while higher β leaves them lighter, as more of the transferred material is lost from the binary altogether. The spread in $M_{2,\mathrm{after\,MT}}$ at fixed initial mass is a direct readout of how much the mass-transfer efficiency shapes the rest of the binary's evolution.

4.7 α_{CE} Constraint

The preceding results establish how the initial binary and the first stable mass-transfer episode determine the systems that reach the second interaction. The final step is to determine how efficiently the common envelope must be ejected for these systems to emerge with the reconstructed post-CE period.

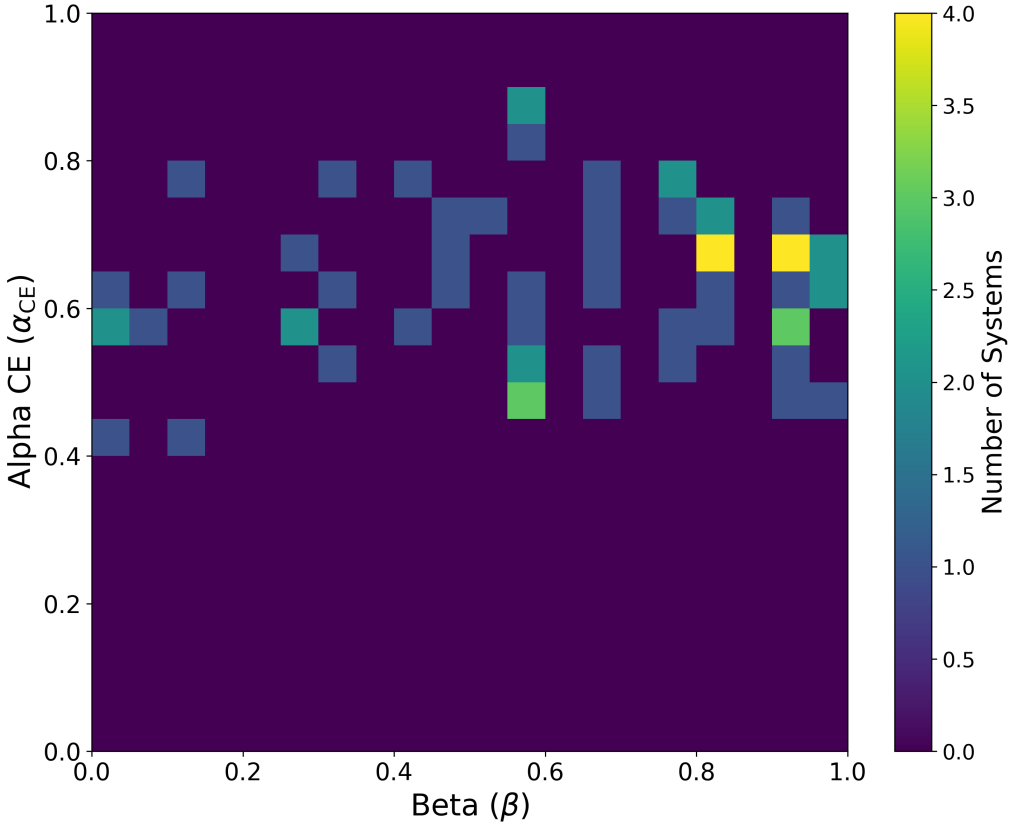


Figure 4.7: Constraint on CE Efficiency for the CD-30 Progenitors

Figure 4.7 shows the distribution of the common envelope efficiency ($\alpha_{\rm CE}$) as a function of the mass-transfer efficiency (β) for the progenitor candidates of CD-30°11223. The successful progenitor systems span a relatively narrow range of common envelope efficiencies with most solutions between $0.4 \lesssim \alpha_{\rm CE} \lesssim 0.8$ and no dependence on the adopted mass-transfer efficiency. Bringing in the β constraints from Figure 4.5 narrows $\alpha_{\rm CE}$ range further, with more than 35% of all successful progenitor candidates clustered within $0.46 < \alpha_{\rm CE} < 0.73$. Overall, moderately efficient common envelope ejection, combined with the preferred range of mass-transfer efficiencies best reproduces the observed properties of CD-30°11223.

4.8 Discussion

The sequence of results provides a consistent picture of the sdB-first pathway. The initial parameter distributions show that successful systems do not arise uniformly across the full grid. Instead, the progenitors are concentrated in a region where the primary can undergo stable Roche-lobe overflow at an appropriate evolutionary stage, while the secondary can accrete enough material to become the more massive star and later evolve into the donor of the common envelope phase. The preferred initial mass ratios, periods, and mass-transfer efficiencies are therefore not independent properties of the final population. They determine whether the binary can pass through the required sequence of two qualitatively different interactions.

The role of β matters here because it links the first and second interactions. The first donor has to be stripped enough to expose a helium burning core, but how much material the secondary retains sets how fast that star grows and when it eventually leaves the main sequence. The models allow a broad range of successful β values, so the sdB-first channel is not tied to one mass-transfer prescription, but the fact that the CD-30 progenitors skew towards higher β tells us the later evolution is sensitive to how much mass and angular momentum was lost during that first interaction. The first mass-transfer phase is not just about making the sdB but also influences the common envelope phase that follows.

This connection explains why the initial-period and β distributions must be considered together. Changing the initial period changes the evolutionary state of the primary when Roche-lobe overflow begins, while changing β changes the mass gained by the secondary and the orbital response to mass transfer. The successful systems therefore occupy a restricted combination of these parameters.

4.8.1 common envelope Efficiency

The common envelope phase provides the second major interaction in the sdB-first evolutionary pathway and determines whether the binary can reach the compact sdB+WD configuration. In the energy formalism adopted here, $\alpha_{\rm CE}$ describes the fraction of the released orbital energy available for envelope ejection. The successful progenitors require values predominantly in the range $0.4 \lesssim \alpha_{\rm CE} \lesssim 0.8$, with a mild preference for intermediate values. These values can be compared with a broad range of efficiencies inferred for other post-common envelope binary populations, spanning white dwarf–main-sequence systems, double white dwarfs, hot subdwarf binaries, and, at the opposite end of the mass scale, the massive-star progenitors of compact-object binaries.

Reconstructions of white dwarf–main-sequence binaries generally favour relatively low common envelope efficiencies. Zorotovic et al. (2010) found that values of $\alpha_{\rm CE} \sim 0.2$–0.3 reproduce most of their observed systems, while Davis et al. (2010) and Davis et al. (2012) found a considerably broader range of efficiencies, with many systems consistent with similarly low values, and identified evidence that the inferred efficiency itself varies with the binary parameters rather than taking a single universal value. De Marco et al. (2011) reached a similar conclusion from an independent sample of post-common envelope systems, including post-asymptotic-giant-branch binaries and the central stars of planetary nebulae, finding that $\alpha_{\rm CE}$ correlates with the binary mass ratio. Monte Carlo population synthesis studies that forward-model the observed SDSS population of white dwarf–main-sequence binaries have independently converged on the same low-efficiency regime (Camacho et al., 2014; Toonen and Nelemans, 2013). Taken together, these results indicate that $\alpha_{\rm CE} \sim 0.2$–0.3 is required to reproduce the bulk of the low-mass post-common envelope population, with only a small number of outlying wide systems requiring additional energy sources beyond the orbital energy alone.

More recent reconstructions extend this picture to other classes of compact companion. Zorotovic and Schreiber (2022) found $\alpha_{\rm CE} \sim 0.2$–0.4 for white dwarf–brown dwarf systems, consistent with the white dwarf–main-sequence result and suggesting that the low-mass, low-efficiency regime persists even as the companion mass drops toward the substellar limit. Scherbak and Fuller (2023) obtained $\alpha_{\rm CE} \sim 0.2$–0.4 for a sample of double white dwarfs and one white dwarf–brown dwarf system, using detailed cooling-age modelling to break the degeneracy between progenitor mass and orbital history that limits single-epoch reconstructions. These results indicate that relatively low efficiencies are commonly inferred for post-common envelope systems involving low-mass donors, although the inferred value remains sensitive to the adopted binary and envelope properties. Studies of subdwarf B binaries provide a closer comparison to the systems considered here, since the sdB progenitor is a stripped core-helium burning star rather than a red giant or evolved main-sequence donor. Han et al. (2002b) and Han et al. (2003) found an efficiency parameter of approximately $\alpha_{\rm H} \sim 0.75$ to reproduce the observed period distribution of short-period sdB binaries. Because their energy prescription includes a fraction of the internal energy of the envelope, this value is not directly equivalent to the standard $\alpha_{\rm CE}$ definition. The corresponding efficiency is approximately $\alpha_{\rm CE} \sim 0.6$ when expressed in the conventional form (Han et al., 2003; Han et al., 2002b). More recently, Ge et al. (2022) investigated the CE evolution of a large sample of 142 hot subdwarf binaries and showed that the inferred efficiency depends on the properties and evo-

lutionary state of the progenitor, with mass-ratio-dependent trends echoing those found by De Marco et al. (2011) for post-AGB systems. Ge et al. (2024) further reconstructed seven short-period sdB+WD binaries and obtained a mean efficiency of $\alpha_{\rm CE} \sim 0.32$, closer to the low values typical of white dwarf–main-sequence binaries than to the higher value found by Han et al. (2003), while also finding evidence for a dependence on the initial mass ratio. Together, these sdB studies show that even within a single class of progenitor, the inferred efficiency spans close to an order of magnitude in methodology-dependent detail, underlining the difficulty of assigning a single characteristic value to the sdB-forming channel.

The values obtained in this work are therefore somewhat higher than those commonly inferred for low-mass white dwarf binaries and the short-period sdB+WD systems considered by Ge et al. (2024), but they remain within the broader range of efficiencies reported for common envelope systems. This difference may be related to the distinct evolutionary history of the CE donor in the present sdB-first channel. Before initiating the common envelope phase, the secondary has gained mass during the preceding stable mass-transfer episode. Its mass, evolutionary state, and internal structure can therefore differ substantially from those of the low-mass giant progenitors commonly considered in white dwarf post-common envelope systems. Since the envelope binding energy depends directly on the structure of the donor, these differences can alter the efficiency required to reproduce a given post-common envelope orbit.

Hydrodynamical and theoretical studies further support the interpretation that $\alpha_{\rm CE}$ should not be regarded as a universal constant. Three-dimensional calculations of low-mass systems have yielded effective efficiencies of order $\alpha_{\rm CE} \sim 0.5$–0.8 in some cases, while studies based on the internal structure of the donor find systematically lower efficiencies for low-mass stars and higher efficiencies for more massive systems (Nandez et al., 2015; Wilson and Nordhaus, 2019, 2020, 2022). Iaconi and De Marco (2019), in a comprehensive comparison of three-dimensional simulations against the full observed population of post-common envelope systems, likewise concluded that $\alpha_{\rm CE}$ derived from simulations is better interpreted as a system-dependent proportionality constant than as a fixed physical efficiency, and that simulated final separations should generally be treated as upper limits given persistent resolution limitations. At the high-mass end of the donor spectrum, this trend becomes extreme: one-dimensional hydrodynamic reconstructions of massive binaries evolving toward compact-object companions require efficiencies approaching, or even exceeding, unity to reproduce the observed post-common envelope orbits (Fragos et al., 2019). Taken together, these studies indicate that the inferred value of $\alpha_{\rm CE}$ depends

on the donor mass, evolutionary state, binary parameters, and the treatment of the envelope binding energy rather than representing a universal property of common envelope evolution.

The $\alpha_{\rm CE}$ values obtained here should therefore be interpreted in the context of the specific binary pathway considered. The relatively high efficiencies compared with many low-mass white dwarf binaries may reflect the more massive and structurally different donor produced by the preceding stable mass-transfer episode. A larger observational sample of sdB+WD systems, together with self-consistent calculations of their progenitor structures, will be required to determine whether the efficiency inferred here represents a characteristic property of the sdB-first channel or arises from the particular systems and envelope-binding prescriptions considered in this work.

4.8.2 Connection to Double-detonation Progenitors

The relevance of the progenitor reconstruction extends beyond reproducing the present-day properties of individual sdB+WD systems. The full MESA grid identifies the region of initial binary parameter space from which compact systems capable of entering the helium-transfer phase can arise. Since the sdB+WD systems considered here are potential progenitors of sub-Chandrasekhar double-detonation Type Ia supernovae, the size and location of this viable region are directly relevant to estimating how frequently this evolutionary pathway may occur.

The present calculations do not by themselves determine a Galactic supernova rate, because such a calculation requires the successful regions of parameter space to be weighted by the underlying distributions of binary masses, mass ratios, orbital periods, metallicity, and binary fraction. Nevertheless, the grid provides the evolutionary selection function needed for such an analysis. In particular, it shows that only a restricted combination of initial parameters passes through stable mass transfer, forms an sdB, survives the subsequent common envelope phase, and produces a compact sdB+WD binary. Applying these constraints within a binary-population synthesis calculation would therefore allow the progenitor formation efficiency of the sdB-first double-detonation channel to be translated into a predicted contribution to the SN Ia rate, following the approach used by Wang et al. (2013) to convert a grid of helium-accreting white dwarf progenitor models into birthrates and delay-time distributions for the closely related helium-ignited sub-Chandrasekhar channel.

So the result of this work is not just a list of individual progenitors, but also a characterization of the binary conditions needed to produce them at all. The 1,035 successful sdB+WD systems define the broader population this evolutionary chan-

nel can produce, and the 53 systems selected against the observed constraints show how that population connects to one specific compact double-detonation candidate. The β and $\alpha_{\rm CE}$ distributions tied to those 53 systems quantify how much the uncertain binary interaction physics shapes that connection. That gives a framework that can be applied to newly discovered sdB+WD systems as they turn up, and, eventually, used to gauge how much this channel contributes to the population of sub-Chandrasekhar Type Ia supernova progenitors.

Chapter 5

Conclusions and Future Directions

5.1 Conclusions

In this thesis, I simulated the evolution of main-sequence binaries toward double-detonation supernovae using MESA, following the alternative pathway in which the sdB forms before the white dwarf through stable mass transfer, so the channel involves only a single common envelope phase. To examine how the evolution depends on the initial configuration, I constructed a grid of simulations varying the primary mass (M_1), mass ratio (q), initial orbital period ($P_{\rm orb}$), and mass-transfer efficiency (β). Of the 106,428 simulations in this grid, 1,035 produced sdB and WD progenitor systems occupying a tightly constrained region of the initial parameter space.

The successful simulations occupy a limited region of parameter space. They cluster at intermediate primary masses, roughly $2.5\,M_\odot \lesssim M_1 \lesssim 5.5\,M_\odot$ and most strongly between 3.2 and $4.8\,M_\odot$, and they strongly favour mass ratios close to unity. This is consistent with binaries of comparable component masses being best able to complete the first stable Roche-lobe overflow phase without entering a premature common envelope phase.

They also cluster at initial orbital periods of about 2 to 6 days, peaking near 4 to 5 days, while the mass-transfer efficiency (β) remains broadly distributed but still clearly shapes which systems survive. Taken together, this indicates that the sdB-first channel is not governed by a single controlling parameter, but by the combined effect of initial mass, mass ratio, orbital period, and mass-transfer efficiency, which together define the narrow region of parameter space where compact sdB and WD binaries can form.

I then used this grid to constrain the progenitors of CD-30°11223, one of two confirmed double-detonation supernova candidates, which answers the **two questions** raised in Section 1.7.

This produced 53 viable progenitors of CD-30 with tightly constrained initial configurations. The primary mass is favoured between 2.8 $M_\odot$ and 4.2 $M_\odot$, with a clear preference near 3.2 $M_\odot$, and, consistent with the stable-mass-transfer requirement established in Chapters 3 & 4, a mass ratio close to unity. For the mass-transfer efficiency, more than 35% of the 53 candidates have $\beta \geq 0.75$, indicating that moderately to strongly non-conservative mass transfer is preferred. They also favour a short initial orbital period, approximately 1.5 to 3.5 days, consistent with early Roche-lobe overflow.

The 53 progenitors also span range of common envelope efficiencies, mostly between $0.4 \lesssim \alpha_{\rm CE} \lesssim 0.8$, and this holds largely regardless of the adopted mass-transfer efficiency. This range sits systematically above the values typically reconstructed for white dwarf and main-sequence post-common envelope binaries, where $\alpha_{\rm CE} \sim 0.2$ to 0.4 is more usual (Davis et al., 2010; Scherbak and Fuller, 2023; Toonen and Nelemans, 2013; Zorotovic et al., 2010). Common envelope evolution remains one of the least understood phases of binary evolution, with substantial uncertainty in the mechanisms behind envelope ejection (Ivanova et al., 2013). The inferred $\alpha_{\rm CE}$ also depends sensitively on how the envelope binding energy is prescribed, including the treatment of internal energy and the location of the core-envelope boundary (Dewi and Tauris, 2000). In addition, CD-30°11223 originates from an intermediate-mass progenitor whose internal structure differs substantially from the low-mass giants that dominate observational post-common envelope binary samples, so both the envelope binding energy and the orbital energy available to expel it differ from the lower mass case. Common envelope efficiency is therefore depends on the masses, evolutionary state, and internal structure of the binary components, and the moderately higher $\alpha_{\rm CE}$ found here may reflect the distinct evolutionary pathway that leads to compact sdB and CO white dwarf binaries.

This interpretation comes with an important caveat. The known population of sdB and WD systems is still small and may not be representative of the intrinsic population. The observed systems skew toward relatively low-mass sdB stars, and selection effects can shift which evolutionary channels are represented in that sample (Han et al., 2003). The higher $\alpha_{\rm CE}$ values found here could therefore partly reflect the currently observed sample rather than a genuine, universal difference in common envelope efficiency. Resolving this will require a larger and less biased population of sdB and WD systems, ideally spanning a wider range of sdB masses.

5.2 Future Directions

5.2.1 Classification of new candidates

A natural extension of this work is the classification of newly discovered double-detonation candidates. The increasing number of compact sdB and WD systems identified by large surveys makes it possible to apply the same binary-evolution framework to systems with measured masses, orbital periods, and atmospheric parameters. By comparing observed systems against evolutionary tracks from a dense MESA grid, one can determine whether a given candidate is compatible with the sdB-first channel, the classical double-degenerate channel, or an alternative evolutionary pathway. This is especially useful for systems with incomplete observational constraints, because the grid can identify which combinations of initial masses, orbital periods, mass-transfer efficiencies, and common envelope efficiencies are physically allowed.

5.2.2 Constraining the double-detonation rate

Another important direction is improving the estimate of the Galactic double-detonation Type Ia supernova rate. The rate depends not only on the number of suitable progenitor systems, but also on the fraction of binaries that pass through the narrow region of parameter space leading to successful sdB and WD formation. The present grid can be combined with binary population synthesis to convert the viable progenitor space into a formation efficiency and, ultimately, a predicted explosion rate. This requires weighting the successful regions of parameter space by realistic distributions of initial binary masses, orbital periods, and mass ratios, and accounting for the survival probability through stable mass transfer and common envelope evolution.

5.2.3 Sensitivity to model assumptions

Beyond the applications discussed above, the grid can be used to assess the sensitivity of the progenitor population to the adopted binary-evolution prescriptions. Since the models were computed at a single metallicity, the present results isolate the influence of the initial masses, orbital periods, mass-transfer efficiency, and common envelope treatment without introducing additional chemical-composition variation. This makes the grid useful for testing how robust the successful parameter region is under alternative assumptions about stable Roche-lobe overflow, non-conservative

mass loss, and common envelope energetics. Such studies would help identify which physical prescriptions dominate the uncertainty budget in the sdB-first channel.

5.2.4 Broader observational use

The same framework can also be applied to other compact sdB and WD binaries beyond the currently known candidates. As new systems are discovered, especially through time-domain surveys and spectroscopic follow-up, the grid can be used to determine whether they are likely progenitors, post-progenitors, or systems that will never reach the helium-transfer phase required for double detonation. The model grid is therefore not only a tool for interpreting individual objects, but also a broader predictive framework for the evolving population of compact binary supernova progenitors.

Bibliography

Angulo, C. and et al. (1999). A compilation of charged-particle-induced thermonuclear reaction rates. *Nuclear Physics A*, 656:3–183.

Bédard, A. (2024). The spectral evolution of white dwarfs: where do we stand? *Astrophysics and Space Science*, 369(4).

Bildsten, L., Shen, K. J., Weinberg, N. N., and Nelemans, G. (2007). Faint Thermonuclear Supernovae from AM Canum Venaticorum Binaries. *The Astrophysical Journal Letters*, 662(2):L95–L98.

Blöcker, T. (1995). Stellar evolution of low- and intermediate-mass stars. ii. post-agb evolution. *Astronomy and Astrophysics*, 297:727–738.

Branch, D. (1998). Type Ia Supernovae and the Hubble Constant. *Annual Review of Astronomy and Astrophysics*, 36:17–56.

Buchler, J. R. and Yueh, W. R. (1976). Compton scattering and radiative transfer in hot stellar matter. *The Astrophysical Journal*, 210:440–454.

Camacho, J., Torres, S., García-Berro, E., Zorotovic, M., Schreiber, M. R., Rebassa-Mansergas, A., Nebot Gómez-Morán, A., and Gänsicke, B. T. (2014). Monte Carlo simulations of post-common envelope white dwarf + main sequence binaries: comparison with the SDSS DR7 observed sample. *Astronomy & Astrophysics*, 566:A86.

Carroll, B. W. and Ostlie, D. A. (2006). *An Introduction to Modern Astrophysics*. Pearson Addison-Wesley, San Francisco, CA, 2nd edition.

Cassisi, S., Potekhin, A. Y., Pietrinferni, A., Catelan, M., and Salaris, M. (2007). Updated electron-conduction opacities: The impact on low-mass stellar models. *The Astrophysical Journal*, 661:1094–1104.

Chandrasekhar, S. (1939). *An Introduction to the Study of Stellar Structure*. Dover Publications, New York.

Chen, X., Han, Z., and Podsiadlowski, P. (2013). Orbital periods of subdwarf B binaries produced by the first stable Roche Lobe overflow channel. *Monthly Notices of the Royal Astronomical Society*, 434(1):186–193.

Chugunov, A. I., DeWitt, H. E., and Yakovlev, D. G. (2007). Coulomb tunneling in dense matter. *Physical Review C*, 76:025805.

Copperwheat, C. M., Morales-Rueda, L., Marsh, T. R., Maxted, P. F. L., and Heber, U. (2011). Radial-velocity measurements of subdwarf B stars. *Monthly Notices of the Royal Astronomical Society*, 415(2):1381–1395.

Cyburt, R. H. and et al. (2010). The jina reaclib database: Its recent updates and impact on type-i x-ray bursts. *The Astrophysical Journal Supplement Series*, 189:240–252.

Davis, P. J., Kolb, U., and Knigge, C. (2010). The effect of common envelope evolution on the visible population of post-common envelope binaries. *Monthly Notices of the Royal Astronomical Society*, 403(1):179–194.

Davis, P. J., Kolb, U., and Knigge, C. (2012). Is the common envelope ejection efficiency a function of the binary parameters? *Monthly Notices of the Royal Astronomical Society*, 419(1):287–303.

D'Cruz, N. L., Dorman, B., Rood, R. T., and O'Connell, R. W. (1996). The Origin of Extreme Horizontal Branch Stars. *The Astrophysical Journal*, 466:359–365.

De Marco, O., Passy, J.-C., Moe, M., Herwig, F., Mac Low, M.-M., and Paxton, B. (2011). On the alpha formalism for the common envelope interaction. *Monthly Notices of the Royal Astronomical Society*, 411(4):2277–2292.

Deshmukh, K., Bauer, E. B., Kupfer, T., and Dorsch, M. (2024). Modelling the am cvn and double detonation supernova progenitor binary system cd-30°11223. *Monthly Notices of the Royal Astronomical Society*, 527(2):2072–2082.

Dewi, J. D. M. and Tauris, T. M. (2000). On the energy equation and efficiency parameter of the common envelope evolution. *Astronomy and Astrophysics*, 360:1043–1051.

Dorman, B., Rood, R. T., and O'Connell, R. W. (1993). Ultraviolet Radiation from Evolved Stellar Populations. I. Models. *The Astrophysical Journal*, 419:596–609.

Fink, M., Röpke, F. K., Hillebrandt, W., Seitenzahl, I. R., Sim, S. A., and Kromer, M. (2010). Double-detonation sub-Chandrasekhar supernovae: can minimum helium shell masses detonate the core? *Astronomy & Astrophysics*, 514:A53.

Fragos, T., Andrews, J. J., Ramirez-Ruiz, E., Meynet, G., Kalogera, V., Taam, R. E., and Zezas, A. (2019). The Complete Evolution of a Neutron-star Binary through a Common Envelope Phase Using 1D Hydrodynamic Simulations. *The Astrophysical Journal Letters*, 883(2):L45.

Fuller, G. M., Fowler, W. A., and Newman, M. J. (1985). Stellar weak interaction rates for intermediate-mass nuclei. ii. a = 21 to a = 60. *The Astrophysical Journal*, 293:1–16.

Ge, H., Tout, C. A., Chen, X., Kruckow, M. U., Chen, H., Jiang, D., Li, Z., Liu, Z., and Han, Z. (2022). The Common Envelope Evolution Outcome – A Case Study on Hot Subdwarf B Stars. *The Astrophysical Journal*, 933(2):137.

Ge, H., Tout, C. A., Webbink, R. F., Chen, X., Sarkar, A., Li, J., Li, Z., Zhang, L., and Han, Z. (2024). The Common Envelope Evolution Outcome. II. Short-orbital-period Hot Subdwarf B Binaries Reveal a Clear Picture. *The Astrophysical Journal*, 961(2):202. arXiv preprint posted Nov. 2023; text cites this as "Ge et al. 2023" – confirm intended year.

Ge, H., Webbink, R. F., Chen, X., and Han, Z. (2010). Adiabatic mass loss in binary stars. i. computational method. *The Astrophysical Journal*, 717:724–738.

Ge, H., Webbink, R. F., Chen, X., and Han, Z. (2020). Adiabatic Mass Loss in Binary Stars. III. From the Base of the Red Giant Branch to the Tip of the Asymptotic Giant Branch. *The Astrophysical Journal*, 899(2):132.

Geier, S., Marsh, T. R., Wang, B., Dunlap, B., Barlow, B. N., Schaffenroth, V., Chen, X., Irrgang, A., Maxted, P. F. L., Ziegerer, E., Kupfer, T., Miszalski, B., Heber, U., Han, Z., Shporer, A., Telting, J. H., Gänsicke, B. T., Østensen, R. H., O'Toole, S. J., and Napiwotzki, R. (2013). A progenitor binary and an ejected mass donor remnant of faint type ia supernovae. *Astronomy & Astrophysics*, 554:A54.

Gentile Fusillo, N. P., Tremblay, P.-E., Gänsicke, B. T., Manser, C. J., Cunningham, T., Cukanovaite, E., Hollands, M., Marsh, T. R., Raddi, R., Jordan, S., Cummings, J. D., Toonen, S., Geier, S., and Barstow, M. A. (2019). A gaia data release 2 catalogue of white dwarfs and a comparison with sdss. *Monthly Notices of the Royal Astronomical Society*, 482(4):4570–4591.

Greggio, L. and Renzini, A. (1990). The ultraviolet upturn in elliptical galaxies and the late stages of stellar evolution. *The Astrophysical Journal*, 364:35–49.

Hall, P. D. and Jeffery, C. S. (2016). Hydrogen in hot subdwarfs formed by double helium white dwarf mergers. *Monthly Notices of the Royal Astronomical Society*, 463(3):2756–2764.

Hamuy, M., Phillips, M. M., Suntzeff, N. B., Schommer, R. A., Maza, J., and Aviles, R. (1996). The Hubble Diagram of the Calan/Tololo Type Ia Supernovae and the Value of H_0. *The Astronomical Journal*, 112(6):2398–2407.

Han, Z., Podsiadlowski, P., Maxted, P. F. L., and Marsh, T. R. (2003). The origin of subdwarf B stars – II. Binary evolution. *Monthly Notices of the Royal Astronomical Society*, 341(2):669–691.

Han, Z., Podsiadlowski, P., Maxted, P. F. L., Marsh, T. R., and Ivanova, N. (2002a). The origin of subdwarf b stars – i. the formation channels. *Monthly Notices of the Royal Astronomical Society*, 336(2):449–466.

Han, Z., Podsiadlowski, P., Maxted, P. F. L., Marsh, T. R., and Ivanova, N. (2002b). The origin of subdwarf B stars – I. The formation channels. *Monthly Notices of the Royal Astronomical Society*, 336(2):449–466.

Heber, U. (2009). Hot Subdwarf Stars. *Annual Review of Astronomy and Astrophysics*, 47(1):211–251.

Heber, U. (2016). Hot Subluminous Stars. *Publications of the Astronomical Society of the Pacific*, 128(966):082001.

Heger, A., Langer, N., and Woosley, S. E. (2000). Presupernova evolution of rotating massive stars. i. numerical method and evolution of the internal stellar structure. *The Astrophysical Journal*, 528:368–396.

Heger, A., Woosley, S. E., and Spruit, H. C. (2005). Presupernova evolution of differentially rotating massive stars including magnetic fields. *The Astrophysical Journal*, 626:350–363.

Hernandez, M. S., Kupfer, T., Belloni, D., and Schreiber, M. R. (2026). From main-sequence binary to blast: MESA modeling of the double-detonation progenitor PTF1 J2238+7430. *Astronomy & Astrophysics*, 708:A108.

Hillebrandt, W. and Niemeyer, J. C. (2000). Type Ia Supernova Explosion Models. *Annual Review of Astronomy and Astrophysics*, 38:191–230.

Hjellming, M. S. and Webbink, R. F. (1987). Thresholds for rapid mass transfer in binary systems. i. polytropic models. *The Astrophysical Journal*, 318:794–808.

Howell, D. A. (2011). Type ia supernovae as stellar endpoints and cosmological tools. *Nature Communications*, 2:350.

Iaconi, R. and De Marco, O. (2019). Speaking with one voice: simulations and observations discuss the common envelope α parameter. *Monthly Notices of the Royal Astronomical Society*, 490(2):2550–2566.

Iglesias, C. A. and Rogers, F. J. (1993). Opacities for enhanced carbon and oxygen mixtures. *The Astrophysical Journal*, 412:752–760.

Iglesias, C. A. and Rogers, F. J. (1996). Updated opal opacities. *The Astrophysical Journal*, 464:943–953.

Irwin, A. W. (2012). FreeEOS: Equation of State for stellar interiors calculations. Astrophysics Source Code Library, record ascl:1211.002.

Itoh, N. and et al. (1996). Neutrino energy loss in stellar interiors. vii. pair, photo-, plasma, bremsstrahlung, and recombination neutrino processes. *The Astrophysical Journal Supplement Series*, 102:411–424.

Ivanova, N., Justham, S., Chen, X., De Marco, O., Fryer, C. L., Gaburov, E., Ge, H., Glebbeek, E., Han, Z., Li, X.-D., Lu, G., Marsh, T., Podsiadlowski, P., Potter, A., Soker, N., Taam, R. E., Tauris, T. M., van den Heuvel, E. P. J., and Webbink, R. F. (2013). Common envelope evolution: where we stand and how we can move forward. *Astronomy and Astrophysics Review*, 21:59.

Jermyn, A. S., Schwab, J., Bauer, E. B., Townsend, R. H. D., and Cantiello, M. (2021). Skye: A modern equation of state for stellar evolution calculations. *The Astrophysical Journal*, 913:72.

Kasen, D., Woosley, S. E., and Heger, A. (2011). Pair instability supernovae: Light curves, spectra, and shock breakout. *The Astrophysical Journal*, 734(2):102.

Koester, D. (2013). White Dwarf Stars. In Oswalt, T. D. and Barstow, M. A., editors, *Planets, Stars and Stellar Systems, Volume 4: Stellar Structure and Evolution*, pages 559–612. Springer, Dordrecht.

Kromer, M., Sim, S. A., Fink, M., Röpke, F. K., Seitenzahl, I. R., and Hillebrandt, W. (2010). Double-detonation Sub-Chandrasekhar Supernovae: Synthetic Ob-

servables for Minimum Helium Shell Mass Models. *The Astrophysical Journal*, 719(2):1067–1082.

Kupfer, T., Bauer, E. B., van Roestel, J., Bellm, E. C., Bildsten, L., Fuller, J., Prince, T. A., Heber, U., Geier, S., Green, M. J., Kulkarni, S. R., Bloemen, S., Laher, R. R., Rusholme, B., and Schneider, D. (2022). Discovery of a double-detonation thermonuclear supernova progenitor. *The Astrophysical Journal Letters*, 925(2):L12.

Langanke, K. and Martínez-Pinedo, G. (2000). Shell-model calculations of stellar weak interaction rates. *Nuclear Physics A*, 673:481–508.

Li, W., Bloom, J. S., Podsiadlowski, P., Miller, A. A., Cenko, S. B., Jha, S. W., Sullivan, M., Howell, D. A., Nugent, P. E., Butler, N. R., Ofek, E. O., Kasliwal, M. M., Richards, J. W., Stockton, A., Shih, H.-Y., Bildsten, L., Shara, M. M., and Bibby, J. (2011). Exclusion of a luminous red giant as a companion star to the progenitor of supernova SN 2011fe. *Nature*, 480(7377):348–350.

Mandal, S., Ghavamian, P., Das, P., Seitenzahl, I. R., Mohamed, S., and Ruiter, A. J. (2026). Deciphering the explosion mechanism of type ia supernovae using their remnants. ii. a deep dive into double detonations with snr 0509-67.5. *The Astrophysical Journal*, 1002(2):155.

Maoz, D. and Badenes, C. (2010). The supernova rate and delay time distribution in the Magellanic Clouds. *Monthly Notices of the Royal Astronomical Society*, 407(2):1314–1327.

Maoz, D. and Graur, O. (2017). Star Formation, Supernovae, and the Delay-Time Distribution of Type-Ia Supernovae. *The Astrophysical Journal*, 848:25.

Maoz, D., Mannucci, F., and Nelemans, G. (2014). Observational Clues to the Progenitors of Type Ia Supernovae. *Annual Review of Astronomy and Astrophysics*, 52:107–170.

Maxted, P. F. L., Heber, U., Marsh, T. R., and North, R. C. (2001). The binary fraction of extreme horizontal branch stars. *Monthly Notices of the Royal Astronomical Society*, 326(4):1391–1400.

Nandez, J. L. A., Ivanova, N., and Lombardi, J. C. (2015). Recombination energy in double white dwarf formation. *Monthly Notices of the Royal Astronomical Society*, 450:L39–L43.

Napiwotzki, R., Karl, C. A., Lisker, T., Heber, U., Christlieb, N., Reimers, D., Nelemans, G., and Homeier, D. (2004). Close binary EHB stars from SPY. *Astrophysics and Space Science*, 291(3):321–326.

Oda, T. and et al. (1994). Rate tables for the weak processes of sd-shell nuclei in stellar matter. *Atomic Data and Nuclear Data Tables*, 56:231–403.

Ostrowski, J., Jermyn, A. S., Paxton, B., Smolec, R., and Schwab, J. (2021). Predictive mixing: A new method for treating convective boundaries in stellar evolution calculations. *The Astrophysical Journal Letters*, 913:L27.

Pakmor, R., Kromer, M., Röpke, F. K., Sim, S. A., Ruiter, A. J., and Hillebrandt, W. (2010). Normal Type Ia Supernovae from Violent Mergers of Carbon-Oxygen White Dwarf Binaries. *Nature*, 463:61–64.

Pakmor, R., Kromer, M., Taubenberger, S., Sim, S. A., Röpke, F. K., and Hillebrandt, W. (2012). Normal Type Ia Supernovae from Violent Mergers of White Dwarf Binaries. *The Astrophysical Journal Letters*, 747(1):L10.

Paxton, B., Bauer, E. B., Schwab, J., Bildsten, L., Blinnikov, S., Brinkman, H. E., Cantiello, M., Dotter, A., Farmer, R., Goldberg, J. A., Marchant, P., Thoul, A., Townsend, R. H. D., Timmes, F. X., and Townsley, D. M. (2019). Modules for experiments in stellar astrophysics (mesa): X-ray bursts, nuclide networks, and energy generation. *The Astrophysical Journal Supplement Series*, 243(2):10.

Paxton, B., Bildsten, L., Dotter, A., Herwig, F., Lesaffre, P., and Timmes, F. X. (2011). Modules for experiments in stellar astrophysics (mesa). *The Astrophysical Journal Supplement Series*, 192(1):3.

Paxton, B., Cantiello, M., Arras, P., Bildsten, L., Brown, E. F., Dotter, A., Mankovich, C., Montgomery, M. H., Stello, D., Timmes, F. X., and Townsend, R. H. D. (2013). Modules for experiments in stellar astrophysics (mesa): Planets, oscillations, rotation, and massive stars. *The Astrophysical Journal Supplement Series*, 208(1):4.

Paxton, B., Marchant, P., Schwab, J., Bauer, E. B., Bildsten, L., Cantiello, M., Dessart, L., Farmer, R., Hu, H., Langer, N., Townsend, R. H. D., Townsley, D. M., and Timmes, F. X. (2015). Modules for experiments in stellar astrophysics (mesa): Binaries, pulsations, and explosions. *The Astrophysical Journal Supplement Series*, 220(1):15.

Paxton, B., Schwab, J., Bauer, E. B., Bildsten, L., Cantiello, M., Dotter, A., Farmer, R., Hu, H., Langer, N., Townsend, R. H. D., Timmes, F. X., and Townsley, D. M. (2018). Modules for experiments in stellar astrophysics (mesa): Convective boundaries, semiconvection, and diffusion. *The Astrophysical Journal Supplement Series*, 234(2):34.

Peters, P. C. (1964). Gravitational radiation and the motion of two point masses. *Physical Review*, 136:B1224–B1232.

Phillips, M. M. (1993). The Absolute Magnitudes of Type IA Supernovae. *The Astrophysical Journal Letters*, 413:L105–L108.

Phillips, M. M., Lira, P., Suntzeff, N. B., Schommer, R. A., Hamuy, M., and Maza, J. (1999). The Reddening-Free Decline Rate Versus Luminosity Relationship for Type IA Supernovae. *The Astronomical Journal*, 118(4):1766–1776.

Piersanti, L., Gagliardi, S., Iben, I., and Tornambé, A. (2003). Carbon-oxygen white dwarfs accreting co-rich matter. i. rotation and helium burning. *The Astrophysical Journal*, 598:1229–1238.

Polin, A., Nugent, P., and Kasen, D. (2019). Observational Predictions for Sub-Chandrasekhar Mass Explosions: Further Evidence for Multiple Progenitor Systems for Type Ia Supernovae. *The Astrophysical Journal*, 873(1):84.

Potekhin, A. Y. and Chabrier, G. (2010). Thermodynamic functions of dense plasmas: Analytic approximations for astrophysical applications. *Contributions to Plasma Physics*, 50:82–87.

Reimers, D. (1975). Circumstellar absorption lines and mass loss from red giants. *Memoires of the Societe Royale des Sciences de Liege*, 8:369–382.

Rogers, F. J. and Nayfonov, A. (2002). Updated and expanded opal equation-of-state tables: Implications for helioseismology. *The Astrophysical Journal*, 576(2):1064–1074.

Ruiter, A. J., Belczynski, K., and Fryer, C. (2009). Rates and Delay Times of Type Ia Supernovae. *The Astrophysical Journal*, 699(2):2026–2036.

Saffer, R. A., Bergeron, P., Koester, D., and Liebert, J. (1994). A Spectroscopic Study of Hot Subdwarf B Stars. *The Astrophysical Journal*, 432:351–374.

Saumon, D., Chabrier, G., and Van Horn, H. M. (1995). An equation of state for low-mass stars and giant planets. *The Astrophysical Journal Supplement Series*, 99:713–741.

Schaefer, B. E. and Pagnotta, A. (2012). An absence of ex-companion stars in the type Ia supernova remnant SNR 0509-67.5. *Nature*, 481(7380):164–166.

Scherbak, P. and Fuller, J. (2023). White dwarf binaries suggest a common envelope efficiency $\alpha \sim 1/3$. *Monthly Notices of the Royal Astronomical Society*, 518(3):3966–3984.

Shen, K. J. and Bildsten, L. (2009). Unstable Helium Shell Burning on Accreting White Dwarfs. *The Astrophysical Journal*, 699(2):1365–1373.

Solheim, J.-E. (2010). AM CVn Stars: Status and Challenges. *Publications of the Astronomical Society of the Pacific*, 122(896):1133.

Spearman, C. (1904). The proof and measurement of association between two things. *The American Journal of Psychology*, 15(1):72–101.

Taubenberger, S. (2017). The extremes of thermonuclear supernovae. In Alsabti, A. W. and Murdin, P., editors, *Handbook of Supernovae*, pages 317–373. Springer International Publishing.

Timmes, F. X. and Swesty, F. D. (2000). The accuracy, consistency, and speed of an electron-positron equation of state based on table interpolation of the helmholtz free energy. *The Astrophysical Journal Supplement Series*, 126:501–516.

Toonen, S. and Nelemans, G. (2013). The effect of common envelope evolution on the visible population of post-common envelope binaries. *Astronomy & Astrophysics*, 557:A87.

Vos, J., Németh, P., Vuckovic, M., Østensen, R., and Parsons, S. (2018). Composite hot subdwarf binaries – I. The spectroscopically confirmed sdB sample. *Monthly Notices of the Royal Astronomical Society*, 473(1):693–709.

Wang, B., Justham, S., and Han, Z. (2013). Producing type Iax supernovae from a specific class of helium-ignited WD explosions. *Astronomy & Astrophysics*, 559:A94.

Webbink, R. F. (1984). Double white dwarfs as progenitors of r coronae borealis stars and type i supernovae. *The Astrophysical Journal*, 277:355–360.

Wilson, E. C. and Nordhaus, J. (2019). The role of convection in determining the ejection efficiency of common envelope interactions. *Monthly Notices of the Royal Astronomical Society*, 485(4):4492–4501.

Wilson, E. C. and Nordhaus, J. (2020). Convection and spin-up during common envelope evolution: the formation of short-period double white dwarfs. *Monthly Notices of the Royal Astronomical Society*, 497(2):1895–1903.

Wilson, E. C. and Nordhaus, J. (2022). Convection reconciles the difference in efficiencies between low-mass and high-mass common envelopes. *Monthly Notices of the Royal Astronomical Society*, 516(2):2189–2195.

Zorotovic, M. and Schreiber, M. R. (2022). Close detached white dwarf + brown dwarf binaries: further evidence for low values of the common envelope efficiency. *Monthly Notices of the Royal Astronomical Society*, 513(3):3587–3600.

Zorotovic, M., Schreiber, M. R., and Gänsicke, B. T. (2010). Post-common envelope binaries from sdss. x. the origin of the white dwarf mass distributions of post-common envelope binaries. *Astronomy and Astrophysics*, 520:A86.

Appendix A

Additional Material

A.1 CD-30 Progenitors List

Table A.1: Initial parameters of the 53 viable CD-30°11223 progenitor candidates.

$M_1\,(M_\odot)$	$M_2\,(M_\odot)$	$P_{\rm init}$ (days)	β
3.60	3.20	2.50	0.75
2.80	2.60	3.00	0.10
2.80	2.80	4.50	0.00
2.80	2.80	5.00	0.00
2.80	2.80	5.50	0.35
2.80	2.80	5.50	0.40
3.00	3.00	3.00	0.35
3.00	3.00	3.00	0.40
3.00	3.00	3.00	0.45
3.00	3.00	3.00	0.50
3.20	3.00	3.00	0.30
3.20	3.00	3.00	0.45
3.20	3.00	3.00	0.75
3.20	3.00	3.50	0.00
3.20	3.00	3.50	0.05
3.20	3.00	3.50	0.15
3.20	3.00	3.50	0.25
3.20	3.00	3.50	0.30
3.20	3.00	3.50	0.35
3.20	3.00	3.50	0.60
3.20	3.00	3.50	0.75
3.20	3.00	4.00	0.55
3.20	3.00	4.00	0.60
3.20	3.00	4.50	0.00

Continued on next page

Table A.1 – continued from previous page

$M_1\,(M_\odot)$	$M_2\,(M_\odot)$	$P_{\rm init}$ (days)	β
3.20	3.00	4.50	0.10
3.20	3.20	4.50	0.55
3.20	3.20	4.50	0.60
3.20	3.20	4.50	0.65
3.20	3.20	5.00	0.60
3.20	3.20	5.00	0.65
3.40	3.00	2.50	0.65
3.40	3.20	3.00	0.45
3.40	3.20	3.00	0.60
3.40	3.20	3.00	0.70
3.60	3.00	2.00	0.70
3.80	3.20	2.00	0.80
3.80	3.40	2.50	0.85
3.80	3.40	2.50	0.90
3.80	3.40	2.50	0.95
3.80	3.60	2.50	0.95
4.00	3.40	2.00	0.90
4.20	3.40	2.00	0.85
4.20	3.40	2.00	0.90
4.20	3.60	2.00	0.95
3.80	3.00	2.00	0.75
3.80	3.60	2.50	1.00
4.00	3.00	2.00	0.80
4.00	3.20	2.00	0.80
4.00	3.20	2.00	0.85
4.20	3.20	2.00	0.85
4.60	3.40	1.50	0.90
4.60	3.40	1.50	0.95
4.60	3.60	1.50	1.00

A.2 Inlist Files for MESA Simulations

A.2.1 Inlist_project

```
&binary_job

   inlist_names(1) = 'inlist1_toOnsetCEevolution'
   inlist_names(2) = 'inlist2_toOnsetCEevolution'

   evolve_both_stars = .true.

/ ! end of binary_job namelist

&binary_controls

   m1 = 2.700d0 ! donor mass in Msun
   m2 = 2.600d0 ! accretor mass in Msun
   initial_period_in_days = 3d0

   ! ============================
   ! ============================
   !     OUTPUT
   ! ============================
   ! ============================

   history_name = "history.data"
   history_interval = 1
   terminal_interval = 20
   write_header_frequency = 20

   ! ============================
   ! ============================
   !  MASS LOSS
   ! ============================
   ! ============================

   limit_retention_by_mdot_edd = .false.

   mass_transfer_alpha = 0.0d0
   mass_transfer_beta  = 0.10d0
   mass_transfer_delta = 0.0d0
   mass_transfer_gamma = 0.0d0

   ! ============================
```

```
! ============================
!  ANGULAR MOMENTUM LOSS
! ============================
! ============================

magnetic_braking_gamma = 4.d0

use_other_jdot_mb = .false.
do_jdot_mb = .false.
include_accretor_mb = .false.
do_jdot_gr = .true.
do_jdot_ml = .true.
do_jdot_ls = .true.
do_jdot_missing_wind = .false.
use_other_extra_jdot = .false.

! Assume that accretion is via a Keplerian disc
do_j_accretion = .false.
use_other_accreted_material_j = .false.

! ============================
! ============================
!  MASS TRANSFER RATE
! ============================
! ============================

mdot_scheme = 'Ritter'

! This avoids stopping the simulation because the WD progenitor fills its
 Roche lobe
!accretor_overflow_terminate = 100.0d0

! ============================
! ============================
!     CIRCULARIZATION
!          AND
!     SYNCHRONIZATION
! The schemes are set in run_binary_extras.f90
! ============================
! ============================

do_tidal_circ = .true.
do_tidal_sync = .true.

sync_mode_1 = 'Uniform'
```

```
   sync_mode_2 = 'Uniform'
   Ftid_1 = 1d0
   Ftid_2 = 1d0
   tidal_reduction = 2.0d0

   ! Relax rotation of star to orbital period
   ! at the beggining of evolution
   !-----------do_initial_orbit_sync_1 = .true.

   ! ============================
   ! ============================
   !  WIND ACCRETION
   ! ============================
   ! ============================

   do_wind_mass_transfer_1 = .true.
   do_wind_mass_transfer_2 = .true.
   use_other_binary_wind_transfer = .false.
   wind_BH_alpha_1 = 1.5d0
   wind_BH_alpha_2 = 1.5d0
   max_wind_transfer_fraction_1 = 1.0d0
   max_wind_transfer_fraction_2 = 1.0d0

   ! ============================
   ! ============================
   !     TIME STEP
   !   [default values]
   ! ============================
   ! ============================

   fm = 0.01d0
   fm_hard = -1d0
   fa = 0.01d0
   fa_hard = 0.02d0
   fr = 0.10d0
   fr_hard = -1d0
   fj = 0.001d0
   fj_hard = 0.01d0
   fe = 0.01d0
   fe_hard = -1d0
   fdm = 0.005d0
   fdm_hard = 0.01d0

/ ! end of binary_controls namelist
```

A.2.2 Inlist_1

```
&star_job

   show_log_description_at_start = .false.
   save_model_when_terminate = .true.
   save_model_filename = 'atOnsetCEevolutionM1.mod'

   ! ============================
   ! ============================
   !     IMPORTANT !!!
   ! Gradually rescale mass of star to new_mass.
   ! Rescales star mass without changing composition
   ! as function of m/mstar.
   ! ============================
   ! ============================

   change_mass_years_for_dt = 1d-2

   ! ============================
   ! ============================
   !     ROTATION
   ! ============================
   ! ============================

   change_rotation_flag = .true.
   new_rotation_flag = .true.

   new_omega_div_omega_crit = 0.01
   set_omega_div_omega_crit = .true.
   relax_omega_div_omega_crit = .true.
   num_steps_to_relax_rotation = 100

   ! ============================
   ! ============================
   !     NUCLEAR NETWORK
   ! ============================
   ! ============================

   auto_extend_net = .true.
   h_he_net = 'basic.net'
   co_net = 'co_burn.net'
   adv_net = 'approx21.net'

/ ! end of star_job namelist
```

```
&eos

/ ! end of eos namelist

&kap

   Zbase = 0.02

/ ! end of kap namelist

&controls

   ! ============================
   ! ============================
   !     STOPPING CONDITION
   ! ============================
   ! ============================

   ! He Flash: onset of sdB phase
   !power_he_burn_upper_limit = 10d0

   ! End of He burning, i.e. central He abundance < e-4
   !xa_central_lower_limit_species(1) = 'he4'
   !xa_central_lower_limit(1) = 0.0001

   ! ============================
   ! ============================
   !     OUTPUT CONTROLS
   ! ============================
   ! ============================

   extra_terminal_output_file = 'log1'
   photo_directory = 'photos1'
   log_directory = 'LOGS1'
   star_history_name = 'history.data'

   profile_interval = 500000
   profiles_index_name = ''
   history_interval = 1
   terminal_interval = 20
   write_header_frequency = 20

   ! ============================
   ! ============================
```

```
!     STRUCTURE EQUATIONS
! ============================
! ============================

energy_eqn_option = 'dedt' ! 'eps_grav'
convergence_ignore_equL_residuals = .true.
okay_to_reduce_gradT_excess = .true.

! ============================
! ============================
!     TIME STEP CONTROLS
! ============================
! ============================

!min_timestep_limit = 1d-12
!max_timestep_factor = 0.d0 !1.2d0

varcontrol_target = 1d-3

!delta_HR_limit = 0.01
!delta_HR_hard_limit = 0.5
!delta_lgL_H_limit = 0.01
!delta_lgL_H_hard_limit = 0.02

! The controls below L_He are needed because of the He flash
!delta_lgL_He_limit = 0.01
!delta_lgL_H_hard_limit = 0.02
!lgL_He_burn_min = 2.0
!delta_lgRho_cntr_limit = 0.05
!delta_lgRho_cntr_hard_limit = 0.1
!delta_lgT_cntr_limit = 0.01
!delta_lgT_cntr_hard_limit = 0.02
!delta_lgT_max_limit = 0.1
!delta_lgT_max_hard_limit = 0.2
!delta_lgTeff_limit = 0.01
!delta_lgTeff_hard_limit = 0.02
!delta_lgL_limit = 0.05
!delta_lgL_hard_limit = 0.1

! ============================
! ============================
!    SOLVER AND TOLERANCE
! ============================
! ============================
```

```
solver_itermin_until_reduce_min_corr_coeff = 25
solver_max_tries_before_reject = 40
max_tries_for_retry = 40
tiny_corr_coeff_limit = 1000
corr_coeff_limit = 0.2d0

ignore_too_large_correction = .true.
ignore_min_corr_coeff_for_scale_max_correction = .true.

use_gold_tolerances = .false.
use_gold2_tolerances = .false.
eps_mdot_factor = 0d0
gold_solver_iters_timestep_limit = 30
gold_iter_for_resid_tol3 = 10
gold_tol_residual_norm3 = 1d-6
gold_tol_max_residual3 = 1d-3

tol_max_correction = 1d-2
tol_correction_norm = 1d-3

max_corr_jump_limit = 1d99
max_resid_jump_limit = 1d99

limit_for_rel_error_in_energy_conservation = 1d-3
hard_limit_for_rel_error_in_energy_conservation = 1d-2
max_abs_rel_run_E_err = 1d99
warn_when_large_rel_run_E_err = 1d0

redo_limit = -1
retry_limit = -1

! ============================
! ============================
!     METALLICITY
! ============================
! ============================

initial_z = 0.02000d0

! ============================
! ============================
!      ROTATION CONTROLS
! ============================
! ============================
```

```
max_mdot_redo_cnt = 300
min_years_dt_for_redo_mdot = 0
surf_omega_div_omega_crit_limit = 0.99d0
surf_omega_div_omega_crit_tol = 0.05d0
mdot_revise_factor = 1.1d0
implicit_mdot_boost = 0.1d0

use_accreted_material_j = .false.
accreted_material_j = 0.d0

! Rotational Mixing
am_nu_visc_factor = 0
am_D_mix_factor = 0.0333333333333333d0
D_DSI_factor = 0
D_SH_factor = 1
D_SSI_factor = 1
D_ES_factor = 1
D_GSF_factor = 1
D_ST_factor = 1

! ============================
! ============================
!    WIND MASS LOSS CONTROLS
! - Reimers: Based on McDonald & Zijlstra (2015, MNRAS, 448, 502)
! - Blocker: Based on Ventura, D'Antona & Mazzitelli (2000, A&A, 363, 605)
!            and Cinquegrana, Joyce & Karakas (2022, ApJ, 939, 50)
! - VW93: It seems to be better for AGB stars
! ============================
! ============================

cool_wind_full_on_T = 9.99d9
hot_wind_full_on_T = 1d10
cool_wind_RGB_scheme = 'Reimers'
cool_wind_AGB_scheme = 'Blocker'
RGB_to_AGB_wind_switch = 1d-4
Reimers_scaling_factor = 0.1000d0
Blocker_scaling_factor = 0.0200d0

! ============================
! ============================
!    MIXING CONTROLS
! ============================
! ============================

mixing_length_alpha = 1.9d0
```

```
MLT_option = 'Henyey'

! ============================
! ============================
! STABILITY AGAINST CONVECTION
! ============================
! ============================

use_ledoux_criterion = .true.
alpha_semiconvection = 1.0d0
thermohaline_coeff = 2

! ============================
! ============================
! PREDICTIVE MIXING
! ============================
! ============================

predictive_mix(1) = .true.
predictive_zone_type(1) = 'any'
predictive_zone_loc(1) = 'core'
predictive_bdy_loc(1) = 'any'
predictive_superad_thresh(1) = 0.005

predictive_mix(2) = .true.
predictive_zone_type(2) = 'any'
predictive_zone_loc(2) = 'surf'
predictive_bdy_loc(2) = 'any'
predictive_superad_thresh(2) = 0.001

! Below is to prevent splitting of the
! core convection zone and/or core breathing pulses
predictive_avoid_reversal(1) = 'he4'

! Below is to avoid smoothing the stabilizing composition jump
! into the convection zone and unphysically causing it to shrink
! (see section 3.2 in Moore, K., & Garaud, P. 2016, ApJ, 817, 54)
num_cells_for_smooth_gradL_composition_term = 0

! ============================
! ============================
! Core overshoot
! ============================
! ============================
```

```
   overshoot_scheme(1) = 'exponential'
   overshoot_zone_type(1) = 'any'
   overshoot_zone_loc(1) = 'core'
   overshoot_bdy_loc(1) = 'top'
   overshoot_f(1) = 0.016
   overshoot_f0(1) = 0.008
   overshoot_mass_full_off(1) = 1.20
   overshoot_mass_full_on(1) = 2.00

/ ! end of controls namelist

&pgstar

/ ! end of pgstar namelist
```

A.2.3 Inlist_2

```
&star_job

   show_log_description_at_start = .false.
   save_model_when_terminate = .true.
   save_model_filename = 'atOnsetCEevolutionM2.mod'

   change_mass_years_for_dt = 1d-2

   change_rotation_flag = .true.
   new_rotation_flag = .true.

   new_omega_div_omega_crit = 0.01
   set_omega_div_omega_crit = .true.
   relax_omega_div_omega_crit = .true.
   num_steps_to_relax_rotation = 100

   auto_extend_net = .true.
   h_he_net = 'basic.net'
   co_net = 'co_burn.net'
   adv_net = 'approx21.net'

/ ! end of star_job namelist

&eos

/ ! end of eos namelist
```

```
&kap

   Zbase = 0.02

/ ! end of kap namelist

&controls

   extra_terminal_output_file = 'log2'
   photo_directory = 'photos2'
   log_directory = 'LOGS2'
   star_history_name = 'history.data'

   profile_interval = 500000
   profiles_index_name = ''
   history_interval = 1
   terminal_interval = 20
   write_header_frequency = 20

   energy_eqn_option = 'dedt' ! 'eps_grav'
   convergence_ignore_equL_residuals = .true.
   okay_to_reduce_gradT_excess = .true.

   varcontrol_target = 1d-3

   solver_itermin_until_reduce_min_corr_coeff = 25
   solver_max_tries_before_reject = 40
   max_tries_for_retry = 40
   tiny_corr_coeff_limit = 1000
   corr_coeff_limit = 0.2d0

   ignore_too_large_correction = .true.
   ignore_min_corr_coeff_for_scale_max_correction = .true.

   use_gold_tolerances = .false.
   use_gold2_tolerances = .false.
   eps_mdot_factor = 0d0
   gold_solver_iters_timestep_limit = 30
   gold_iter_for_resid_tol3 = 10
   gold_tol_residual_norm3 = 1d-6
   gold_tol_max_residual3 = 1d-3

   tol_max_correction = 1d-2
   tol_correction_norm = 1d-3
```

```
max_corr_jump_limit = 1d99
max_resid_jump_limit = 1d99

limit_for_rel_error_in_energy_conservation = 1d-3
hard_limit_for_rel_error_in_energy_conservation = 1d-2
max_abs_rel_run_E_err = 1d99
warn_when_large_rel_run_E_err = 1d0

redo_limit = -1
retry_limit = -1

initial_z = 0.02000d0

max_mdot_redo_cnt = 300
min_years_dt_for_redo_mdot = 0
surf_omega_div_omega_crit_limit = 0.99d0
surf_omega_div_omega_crit_tol = 0.05d0
mdot_revise_factor = 1.1d0
implicit_mdot_boost = 0.1d0

use_accreted_material_j = .false.
accreted_material_j = 0.d0

am_nu_visc_factor = 0
am_D_mix_factor = 0.0333333333333333d0
D_DSI_factor = 0
D_SH_factor = 1
D_SSI_factor = 1
D_ES_factor = 1
D_GSF_factor = 1
D_ST_factor = 1

cool_wind_full_on_T = 9.99d9
hot_wind_full_on_T = 1d10
cool_wind_RGB_scheme = 'Reimers'
cool_wind_AGB_scheme = 'Blocker'
RGB_to_AGB_wind_switch = 1d-4
Reimers_scaling_factor = 0.1000d0
Blocker_scaling_factor = 0.0200d0

mixing_length_alpha = 1.9d0
MLT_option = 'Henyey'

use_ledoux_criterion = .true.
```

```
   alpha_semiconvection = 1.0d0
   thermohaline_coeff = 2

   predictive_mix(1) = .true.
   predictive_zone_type(1) = 'any'
   predictive_zone_loc(1) = 'core'
   predictive_bdy_loc(1) = 'any'
   predictive_superad_thresh(1) = 0.005

   predictive_mix(2) = .true.
   predictive_zone_type(2) = 'any'
   predictive_zone_loc(2) = 'surf'
   predictive_bdy_loc(2) = 'any'
   predictive_superad_thresh(2) = 0.001

   predictive_avoid_reversal(1) = 'he4'

   num_cells_for_smooth_gradL_composition_term = 0

   overshoot_scheme(1) = 'exponential'
   overshoot_zone_type(1) = 'any'
   overshoot_zone_loc(1) = 'core'
   overshoot_bdy_loc(1) = 'top'
   overshoot_f(1) = 0.016
   overshoot_f0(1) = 0.008
   overshoot_mass_full_off(1) = 1.20
   overshoot_mass_full_on(1) = 2.00

/ ! end of controls namelist

&pgstar

/ ! end of pgstar namelist
```

Statutory Declaration

I declare that I have authored the Master's thesis independently and have not used any aids other than those specified. I have clearly labelled all passages that are taken from other works in terms of wording or meaning as borrowed material, stating the exact source in each case. I confirm that I have not already submitted this thesis in the same or a similar version in another examination procedure.

If electronic aids based on generative artificial intelligence (gAI) were used in the course of the preparation of this Master's thesis, I confirm that my own work was the main focus and that complete documentation of all aids used is available in accordance with good scientific practice. I am responsible for any incorrect or distorted content, incorrect references, violations of data protection and copyright law or plagiarism generated by the gAI.

I agree that the Master's thesis may be published.

Hamburg, 3 September 2026



Place, date

Signature